Univerzita Karlova

Přírodovědecká fakulta

Geologie - klasická archeologie

Viktória Cseryová

Strusky ze zpracování mědi na lokalitě Al Salili, 2000 př. n. l., Sultanát Omán

Slags from copper processing at the Al Salili site, 2000 BC, Sultanate of Oman

Bakalářská práce

Vedoucí práce:

RNDr. Jakub Trubač Ph.D.

Konzultanti:

Prof. RNDr. Vojtěch Ettler Ph.D.,

Ing. Roman Garba Ph.D.

Praha, 2022

Charles University

Faculty of Science

Geology

Geology – Classical archaeology

Viktória Cseryová

Slags from copper processing at the Al Salili site, 2000 BC, Sultanate of Oman

Strusky ze zpracování mědi na lokalitě Al Salili, 2000 př. n. l., Sultanát Omán

Bachelor´s thesis

Supervisor:

RNDr. Jakub Trubač Ph.D.

Consultants:

Prof. RNDr. Vojtěch Ettler Ph.D.,

Ing. Roman Garba Ph.D.

Prague, 2022

Abstrakt

Hutnictví v arabském světě bylo vždy známa. V současné době probíhá na území Ománu výzkum, který by měl odhalit další podrobnosti o rudných ložiscích, která byla využívána k výrobě starověkých artefaktů. Cílem této práce je popsat vhodné metody, které nám umožní nahlédnout do tajů zpracování ložisek mědi na lokalitě al-Ṣalaylī v Ománu.

Tato bakalářská práce se zabývá celkovým chemickým a mineralogickým složením starověkých měděných metalurgických strusek z lokality al-Ṣalaylī v Ománu (Jihovýchodní Arábie). Tyto strusky lze pravděpodobně datovat v rozmezí do pozdní doby bronzové, rané doby železné až středního islámského období.

Cílem této práce bylo charakterizovat odebranou strusku kombinací analýz jako optická a skenovací elektronová mikroskopie, rentgenová difrakční analýza a elektronová mikroanalýza, aby bylo možné určit složení a popsat minerální fáze ve strusce a určit podmínky pravěkého metalurgického procesu. Výsledky analýzy ukázaly, že vzorky byly kusy kuželové strusky a pecní strusky z výroby mědi. Zkoumané strusky jsou složeny převážně z Ca-Fe-Mg olivínu a klinopyroxenu vyplněného křemičitým sklem a spinelem. Měď se vyskytuje buď jako kovová fáze s drobnými zrnky Cu, nebo je vázána v sulfidech, které tvoří inkluze obklopené silikátovou matricí. "Furnace" struska je složena převážně z oxidů železa a mědi se zbytky silikátového skla a olivínu. V případě "tapping" strusek z byl proces krystalizace a tuhnutí relativně rychlý v závislosti na tvaru krystalů olivínu ve strusce (nejpomalejší kolem 5 °C za hodinu, nejrychlejší 40-80 °C za hodinu). Dosažená teplota, kdy došlo k tavení rudy, se vzhledem k objemovému chemickému složení strusek v ternárním diagramu SiO2 - CaO - FeO pohybovala kolem 1100-1200 °C, což je běžná teplota pro procesy tavení měděných strusek. Závěrem lze říci, že předběžný výzkum na této lokalitě ukázal pokročilé metalurgické procesy a autor této práce se chce věnovat další charakterizaci těchto strusek v navazující diplomové práci.

Klíčová slova: struska, al-Ṣalaylī, starověká výroba mědi, archeometalurgie, tavení mědi, jihovýchodní Arábie

Abstract

Metallurgy in the Arab world has always been famous. Research is currently underway on the territory of Oman, which should reveal more details of the ore deposits that were used for the production of ancient artifacts. This work aims to describe appropriate methods that will allow us to gain insight into the secrets of processing copper deposits at the al-Ṣalaylī site in Oman.

This bachelor thesis deals with the overall chemical and mineralogical composition of ancient copper metallurgical slags from the al-Ṣalaylī site in Oman (South-eastern Arabia). These slags can probably be dated in range from the Late Bronze Age, Early Iron Age to Middle Islamic Period.

This work aimed to characterize collected slag using a combination of optical and scanning electron microscopy analysis, X-ray diffraction analysis and electron microanalysis, it has been possible to determine the composition and describe the mineral phases in the slag and to determine the conditions of the prehistoric metallurgical process. The results of analysis indicated that the samples were pieces of tapped slag and furnace slag from a production of copper. Examined slags are mainly composed from Ca-Fe-Mg olivine and clinopyroxene filled with silicate glass and spinel. Copper either occurs as metallic phase with small Cu grains or is bound in sulphides, which form inclusions surrounded by the silicate matrix. Furnace slag is mainly composed from iron and copper oxides with silicate glass and olivine residues. In case of tap slags was crystallisation and solidification process relatively quick depending on shape of olivine crystals in slags (slowest around 5 °C per hour, fastest 40-80 °C per hour). Reached temperature when occurred ore melting, due to slags bulk chemical compositions in the SiO2 – CaO – FeO ternary diagram, was around 1100–1200 °C, which is normal temperature for copper slag smelting processes. Content of copper was different in examined slags which can indicate different techniques and periods when it was manufactured. In conclusion, preliminary research at this site has shown advanced metallurgical processes and the author of this thesis intends to further characterise these slags in a follow-up thesis.

Key words: slag, al-Ṣalaylī, ancient copper production, archaeometallurgy, copper smelting, South-eastern Arabia

Acknowledgement

I would like to thank my supervisor, RNDr. Jakub Trubač Ph.D., for his guidance and valuable suggestions during the process of writing my thesis. I am grateful also to my consultants Prof. RNDr. Vojtěch Ettler Ph.D., and Ing. et Mgr. Roman Garba Ph.D. Also, I would like to thank Prof. Paul Yule for providing me with help, Mgr. Pavel Škácha Ph. D. for arranging photography, and my family and friends for support during work on my thesis.

Furthermore, I would like to thank the analytical laboratories of the Institute of Geosciences, in particular: Ing. Věra Vonásková, Lenka Jílková (silicate analysis, trace elements), doc. Petr Drahota and Mgr. Pavel Škácha Ph.D. (XRD), Mgr. Martin Racek Ph. D. (SEM, EPMA), Mgr. Jan Kulhánek (optical microscope).

Prohlášení:

Prohlašuji, že jsem závěrečnou práci zpracovala samostatně a že jsem uvedla všechny použité informační zdroje a literaturu. Tato práce ani její podstatná část nebyla předložena k získání jiného nebo stejného akademického titulu.

V Praze, 29. 8. 2022 Viktória Cseryová

Contents

1. Introduction

The submitted bachelor thesis is divided into two parts. The first part briefly introduces the geological setting in Oman and also summarised the archaeological context and historical significance of copper ore mining in the Arabian Peninsula, which is in the nature of complimentary research. The second part of the thesis presents the analytical techniques that have been used to identify the slag types unambiguously and reliably, including their chronological classification and obtained results.

From the point of view of ancient copper mining, the site of al-Ṣalaylī (Sultanate of Oman) is one of the most archaeologically important source areas of copper ore used for smelting and the copper ingots were exported to ancient Mesopotamia. The evidence of metallurgy activities starting from the Late Bronze Age 2000 BCE. The bachelor thesis aim is to perform chemical and mineralogical analysis of slag materials from this locality using a combination of methods (X-ray fluorescence, X-ray diffraction, optical and electron microscopy, electron microprobe) and compare the obtained results with analogous slags from Cu processing in similar localities in the Middle East or Europe.

Various analyses have been carried out on the collected material, including phase composition analysis using X-ray diffraction, trace element analysis and silicate analysis for bulk composition, quantitative chemical analysis of individual phases using spectrometers on electron microprobe, and carbon dating. Based on the composition of the slags and the composition and shape of the crystals, the melting temperature and solidification rate was determined.

Slags are often viewed in two ways; the archaeological view, which often involves only description and typology according to their shape, and the geochemical view, which combines different analyses and more exact approaches. As reported in an article focusing on slags as early as 1976: “The purpose of the investigation is twofold first, to gain insights into the processes which had produced these slags; and second, to illustrate the type of approach that can be taken in technical work in archaeological problems… It should be stressed, however, that in all archaeological work samples should be characterised by as many properties as can be measured in order to verify as broadly as possible the internal consistency of any interpretation” (Franklin et al., 1976).

The main questions that will be analysed in this thesis:

1. How did copper mining affect European culture in terms of artifacts?

2. How large were the copper deposits that could be exploited?

3. Why is it important to use multiple analytical methods when researching archaeological metallurgical areas?

4. What can the dating of the slag from the al-Ṣalaylī area bring?

___ Current state of knowledge

2. Geological settings, and natural resources in Oman, al-Ṣalaylī

Al-Hajar Mountains in the North Sharqiyah region (Khan, 2002) occupy South-eastern Arabia which consists of major geographical features such as the sea, deserts, and mountains chaining in northern Oman roughly 700 km long (Garba, 2014; Ghazanfar, 1992) rising up to the highest point, Djebel Shams, 3009 m above sea level. Also known as the "Oman Mountains" they separate the low humid coastal plain of Oman from the high hot and dry desert plateau and lie 50-100 km inland from the Gulf of Oman. They create the highest mountain range in the eastern Arabian Peninsula with its unique distinct ecoregion and also the highest point with wildlife in eastern Arabia (Garba, 2014). Mountains are divided by gorges, which forms *wadis* that are usually richer in vegetation (Ghazanfar, 1992). In history, these few elevation gaps in the whole mountain range made important communication and transport passages (Garba, 2014). Aquifers in which Oman has a large amount of water were replenished thousands of years ago when climate conditions prevailed (Giardino 2017). The present-day Oman is well known for droughts and receives limited rainfall that contributes to water supply shortages, this region of Hajar mountains is arid with irregular but seasonal rainfall (Ghazanfar, 1992), but it changes dramatically within the region to another (Giardino, 2017). Generally, the rainfalls take place more often in the mountains (Giardino, 2017). Winter rains occur from November to April in centre and north of Oman, while seasonal summer monsoon occurs from June to September in the southern parts of country causing temperature changes (Giardino, 2017). *Wadi* basins are fed by a large, diffused system of water-bearing layers in the foothill area, which is supplied by atmospheric precipitations (Giardino, 2017). The presence of vegetation along the wadis could favour ancient metalworkers.

2.1. Geological settings

The studied area consists of various allochthonous units including the rocks of magmatic ophiolitic sequence thrusted over the pre- and post-Hercynian (par-)autochthonous basements. Several Cu-rich deposits were described from the ophiolitic magmatic rocks (**Fig. 1**; Scharf et al., 2021).

2.1.1. Semail Ophiolite

In the Oxford Dictionary of Geology and Earth Science (Allaby, 2013) is an ophiolite defined as a "Sequence of rock types, consisting of deep-sea sediments lying above basaltic pillow lavas, dykes, gabbro, and ultramafic peridotite. Some are the remnants of main oceanic crust, others of crust formed in back-arc basins."

Such an ophiolitic complex was created during the separation of the old continents Laurasia and Gondwana through a sequence of fast oceanic spreading and supra-subduction zone volcanism within the Tethys Ocean, which was followed by the breakup of Pangea. The opening of the Tethys Ocean lasted only a few million years, followed by the closure during the middle-upper Cretaceous times (Hacker et al., 1996; Searle et al., 1999; Dilek and Furnes, 2009; Rioux et al., 2013). The resulted Ophiolitic complex was not subducted as it usually for continent-ocean crust collisions, but it was obducted, thrusted up on the Arabian craton and resulted into the obduction, thrusting the Semail Ophiolite Complex (SOC) over the Arabian continental plate basement (Siwitskis, 2019). During the obduction was active just small regional doming and local thrusting, so it did not result in a major structural reworking of the ophiolite units and most primary lithostratigraphic relations are well preserved (Gilgen, 2014). The Semail Ophiolite Belt is a large intact thrust slice of SOC, covering 8–12 km of upper mantle peridotites, where most of the mantle sequence is composed of commonly serpentinized harzburgite, and 4–7 km of oceanic crustal rocks (Partington, 2009). Accumulations of copper ore accessible to ancient miners in Oman can be divided into two categories (Moorey, 1999), both formed through the activity of hydrothermal processes (Pracejus and Scharf, 2020), it can be either veins in gabbro and peridotite with Cu-mineral assemblage of cuprite, malachite, brochantite, azurite, and chrysocolla, or massive sulphide deposits of chalcopyrite, covellite, and chalcocite (Weeks, 2003a).

2.1.2. VMS copper-gold mineralisation in Oman

The type of Volcanic-associated massive sulphide (VMS) found in Semail Ophiolite Belt occur sporadically within the extrusive sequence (Gilgen, 2014) and are believed to have formed on a spreading ridge in an island ring, supra-subduction setting, around active hydrothermal vents, and black smoker deposits (Partington, 2009). More than 150 Volcanogenic Massive sulphide deposits of Cyprus type and many smaller sulphide mineralisation clusters within oceanic volcanics stretches over 500 km (Pracejus and Scharf, 2020). The deposits are formed by lenticular ore body, which is commonly tectonically reworked, and the underlying stockwork mineralisation of the feeder system (Pracejus and Scharf, 2020). Several VMS deposits in Oman are well exposed in the mountain terrain of the ophiolite, but many are partly buried (Gilgen, 2014). Precisely these VMS deposits are major sources of copper (Partington, 2009) and many other important minerals.

2.1.3. Veins in gabbro and peridotite

Many authors generalize the vein systems enriched by Cu-mineralization as the VMS: Cyprus type, but a lot of slag heaps and smelting sites are located in gabbroic and peridotitic prospects, where the veins hydrothermal activity is commonly connected with the successive orogenetic movements (Manhfound and Beck, 1997). This leads to the formation of epigenetic sulphide deposits in the ophiolite rocks, mainly the Fe- and Cu-sulphide rich mineralization hosted by mid-ocean ridge basalts (commonly forming pillow lavas), sheared gabbro, and peridotite (serpentinized) or bounded to the dikes of jasperoid (quartzite) and silica veins passing through the ophiolite (Manhfound and Beck, 1997). The peridotite is mylonitized along shear zones and the gabbroic rocks locally are argilitically altered (Manhfound and Beck, 1997). The origin of many larger wadis are the major fractures, and principal copper mineralisation zones occur in these Wadis and has similar trend (Howari et al., 2022). In the eastern part of Hajar Mountains, near to Ibra, within the mantle rocks (dominantly harzburgites) occur copper-rich ore deposits (Pracejus and Scharf, 2020).

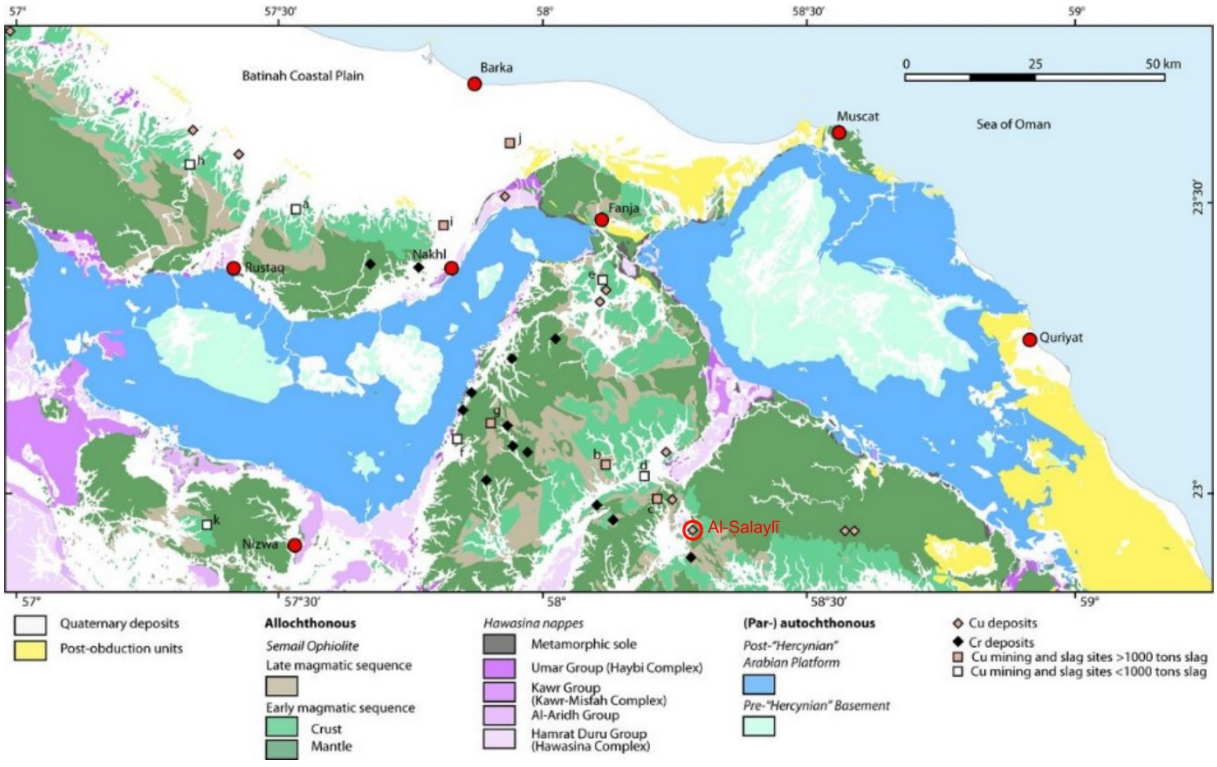

Figure 1: Geological map with marked copper deposits and copper mining as well as slag fields sites (after Scharf et al., 2021)

2.1.4. Raw material sources

More than 150 copper ore deposits are identified by geological survey in South-eastern Arabia (Weeks, 2003a), with major deposits showed at **Fig. 2**. Since Bronze Age Umm an-Nar period (2500-2000 BC) until recently have been copper mined in Oman (Partington, 2009), which produced enormous amounts of waste products (Pracejus and Scharf, 2020). Products of copper oxidation formed by reaction with oxygen creating green coloured oxidized ores such as cuprite, malachite, azurite, chrysocolla and together with native copper (Hauptmann, 2007) have been mined and collected for further processing (Weisgerber, 2007b). The al-Ṣalaylī sites lie 2 km southeast of the Ǧebel al-Ḥawrah mountain (Gaudielo and Yule, 2019). The location of metal production in al-Ṣalaylī is closely related to the geology of this region and its researched area, geologic history, and the associated availability of copper (Sivitskis, 2019). The backbone of mountains in Northern Oman are ophiolitic belts on which is embedded in (Garba, 2014). In South-eastern Arabia is the sulphidic ore, mainly represented by chalcopyrite, the main source of copper (Garba, 2014). The reportedly vertical, 1m thick main copper vein running in a north-north-westerly/south-south-easterly direction along fault between peridotites (harzburgite, lherzolite, and minor dunite in cumulate mineral zones) with length of approximately 755 m. Gallery follows this vein with old working space around 230 m long (Yule, 2021a). The mine is irregularly shaped as we can see thanks to at least 13 cave-ins and well-like deep soundings in the hollowed out vein. The second large vein is located 40 m north east, exposed in a 6 m wide deep trench. The 10 m or even deeper gallery along this vein is exposed and collapsed (Yule, 2021a) Another search gallery lies distant from the main mine and the smelting site with the most accessible entrance is 130 m away from the edge of the "Persian village" at **Fig. 3** (Yule, 2021a). At the place, in the past incorrectly described as "Musfa," which now is assumed to lie 3.5 km to the NNW, was located collapsed gallery of copper mine (Gaudiello and Yule, 2019). There is also a traceable exploration of 115m to 140 m long copper vein, about 130 m to the west distant from the main shear zone was located a search gallery which the miners made (Gaudiello and Yule, 2019).

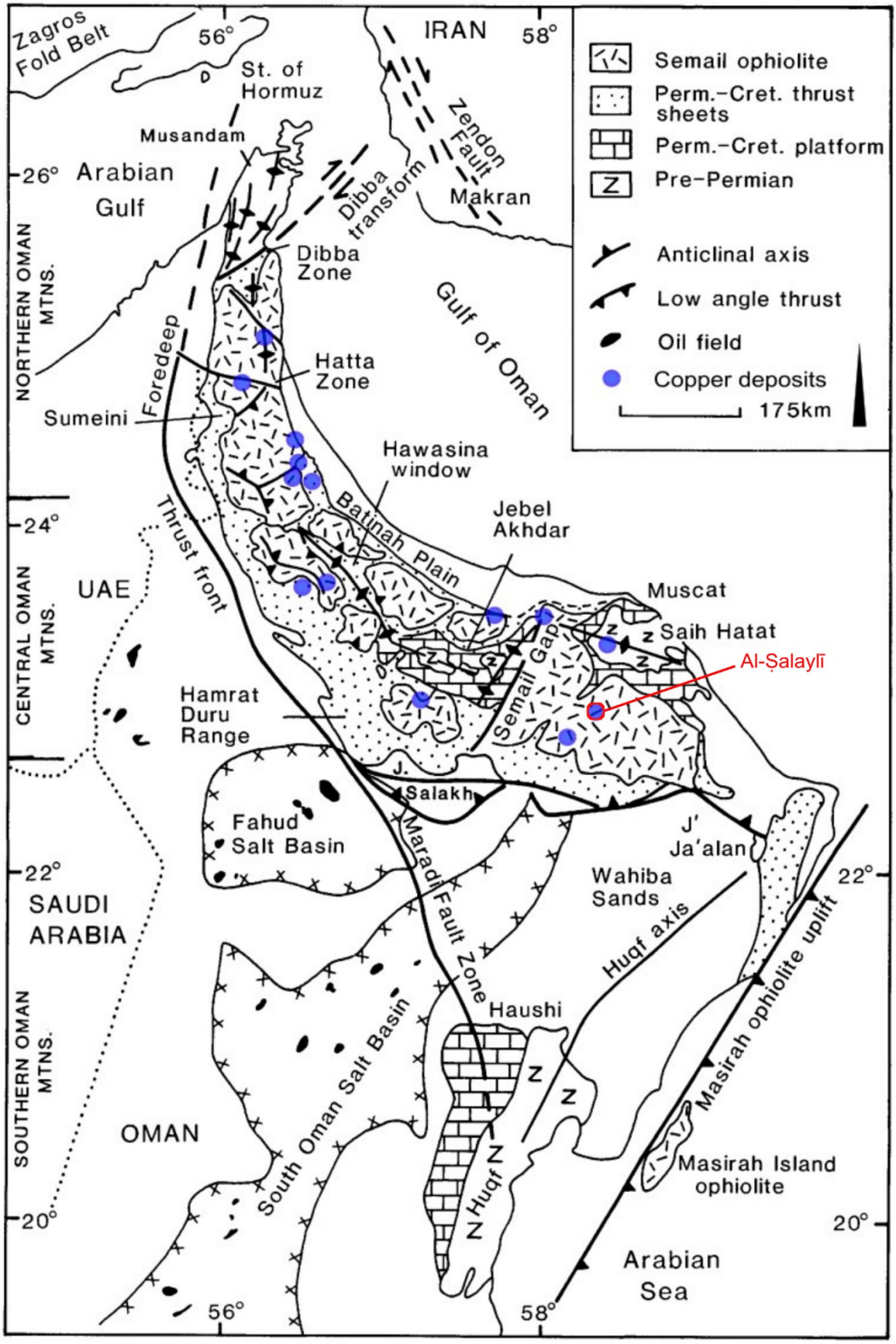

Figure 2: Structural sketch map of the Oman mountains with highlighted major copper deposits in South-eastern Arabia (modified after Glennie et al., 1974; Clarke, 1988; Robertson et al., 1990; Weeks, 2003a; Schreiber, 2007; Garba, 2014)

2.2. Natural resources of energy for metallurgy

The crucial part of the existence of local metallurgical activities is not only the source of ore deposits (Garba, 2014), but also for extraction of metallic copper during the smelting process it is necessary to reach the high required temperature (1100–1200 °C) and reduced atmosphere rich in carbon monoxide rather than oxygen (Garba, 2014; Dungworth, 2012). To reach such a high temperature it is essential to have a large quantity of wood or charcoal (Weeks, 2003) from local sources (Garba, 2014). To produce that number of slags observed during the periods is necessary quantity of fuel, also wood is used in many steps from mining (for example mine support, torches) to smelting (Hauptmann, 2007). The sandy desert landscape, as we know Oman nowadays, is the result of heavy deforestation by large-scale wood logging complemented by gradual climate change (Garba, 2014; Weeks, 2003a). Climate and environment conditions during the EIA and earlier periods were different, which was more suitable for forest vegetation, with an increase in annual rainfall and a significant decrease in temperature (Almazroui, 2012). That allowed to collect rainfall water and held it until it was relieved into semi-permanent streams or even permanent rivers (Garba, 2014). Al-Ṣalaylī's preservation results from fluctuating water availability, which interdicts permanent habitation (Yule, 2021a). In a field report from 2021 (Yule et al., 2021b) it is written that water resources are greater than previously presumed (close to al-Ṣalaylī site 1), even documented with photography of a running waterfall at the site. Two streams were active even during the summer heat (Yule et al., 2021b). A map (**Fig. 3**) from Paul Yules (2021a) papers shows a water stream flowing along the entire al-Ṣalaylī site, but it is later mentioned that there was a lack of water and fuel in the EIA and middle Islamic period and that it is difficult to understand how this site worked and was able to operate based on current knowledge about water resources (Yule, 2021a). In the 3rd millennium BCE were common furnaces powered by wind (instead of using blowpipes to supply an extra air to the smelting hotspots), where natural wind runs via the t*uyères* in the inside segment of reaction vessels, or in the case of natural draught furnaces, where the wind is fluctuating trough the chimney (Rehder, 1994; Hauptmann, 2007; Ben-Yosef, 2008; Garba, 2014). These types of wind-powered or natural draught furnaces played large role in development of metallurgy, but they had not been automatically recognised as such (Hauptmann, 2007). For the functionality of such furnaces, they need to have an exposed location, usually on the top of the hills or cliffs, in order to use wind (Hauptmann, 2007). Furnaces using natural draft had longer melting times, roughly in the range of 30–100 hours (Petrík and Mihok, 2007).

3. Archaeology of al-Ṣalaylī site

During the 19th century, the search for copper mines has started by commercial geologists and pioneer archaeologists in eastern Oman (Yule, 2021a). This gave birth to the linking the owners/builders of hut tombs EIA copper producers in al-Ṣalaylī (Yule, 2021a).

One of the best-preserved EIA burial sites are the al-Ṣalaylī cemeteries with 245 tombs along with other localities such as al-Khadwdh, Hor al-Dhabʿ (145 tombs) and Biad al-Maʿdin (118 tombs). Hut tombs **(Fig. 3)** are dated by their architecture and a finding situation to the EIA (Yule et al., 2021b). The main funerary structures encountered are hut tombs, niche graves and cylindrical tombs which are more recent (Yule et al., 2021b). The al-Ṣalaylī locality consists of the ancient mine, copper smelting production and EIA settlement which lies outside of the main valley to the northeast (Yule et al., 2021b). The development of a pottery mostly made by hand during the EIA in South-eastern Arabia shows a significant number of basic pottery shapes, ornamental elements, and manufacturing techniques as well as compositional syntax (Benoist, 2000; Yule, 2021a). Rough dating can be given by stone vessels and lids, but they are rarely found in the particular period burial structures (Yule, 2001, 2021a).

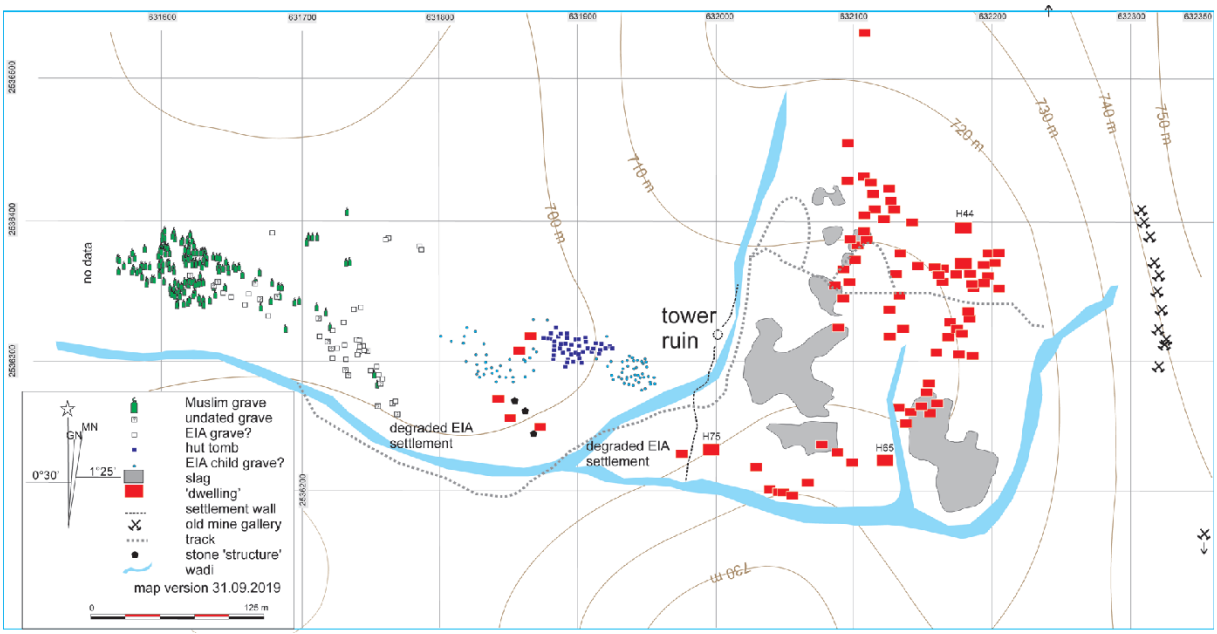

Figure 3: Plan of the easternmost sites of the al-Ṣalaylī archaeological zone showing the site 1 (centre) with hut tomb cemetery (navy blue) surrounded by earth burials of child (light blue dots), green shows Muslim graves, the slag fields (grey), east is "Persian village" including the (red rectangle) buildings - the Islamic settlement (at right) and the abandoned mine (mine symbol), (Yule, 2021)

3.1. Hut tombs

A major feature of the south-eastern Arabian archaeology are tombs. Hut tombs can be important and helpful for us because of their construction and murals can contribute slags and thangs to knowing the era of the hut tomb, we can frame dates including slag. Walls of hut tombs consist mainly of broken unformatted stones about head size, often rounded from Wadi able to stand heavy winter rains during the centuries (Yule, 2021a). The team of archaeologist behind the field report (Yule et al., 2021b) compared the regionally different kinds of tomb entrances. In north-eastern Oman, rarely could we determine a clear hut tomb entrance. The deposit of the deceased was for such tombs from above (Yule et al., 2021b). At al-Ṣalaylī the tombs lie scattered in four spatial groups. Entrances to hut tombs tend to point Wadi down slope allowing of view opening wadi (Yule, 2021a; 2021b). Later EIA earth graves have the same orientation (Yule, 2021a). Small EIA sites are preserved and are showing a smaller number of disturbances than large ones (Yule et al., 2021b). By far, the country's largest accumulation of hut tombs lies in the Batina foothills. Tombs are overwhelmingly the major feature of the south-eastern Arabian archaeology (Yule et al., 2021b).

3.2. Al-Ṣalaylīs slag fields

Place named "Musfa," in fact Al-Musfah, comprises an area of several square km and it is unclear where exactly were mines located, on the North or South side of the Ǧebel al-Ṣalaylī (Gaudiello and Yule, 2018). The smelting sites "Gebel Saleli" and "Musfah" in Oman are merged into one as "prospection site 45" due to Hauptmann (1985), where on locality "Musfah site 45" is the occurrence of the heap with 500 tons of early Islamic slags (22.9333333, 58.2666667), and on locality "Gebel Saleli site 45" was recognised 35.000 tons of Bronze Age to early and middle Islamic slags (22.9333333, 58.2666667) as interpreted by Yule (2021a) site "45 Musfa" contains >1000 tons of copper slag.

Al-Ṣalaylī copper slag fields (**Fig. 23**) were mainly damaged by prospect of mining companies attempting to determinate the quantity of slag available (Gaudiello and Yule, 2019). The slag fields are situated at the eastern end of the valley, west of the mine and are deeper towards the west and thinner towards the north (Yule, 2021a). Slag heaps at al-Ṣalaylī site are deep approximately 1.3 m or even deeper mostly from early or probably middle Islamic date (Yule et al., 2021b). In the different places slag fields vary highly in appearance (Yule, 2021a). We can delimit four areas with unclear boundaries, which can overlap: great density slag accumulations with large and medium sized fragments; slag combined with scattered stones;

slag combined with ruined stone structures; crushed slag (Yule, 2021a). Near to the mine entrance in the valley lie a large slag field, hut tomb and settlement of metal workers (Gaudiello and Yule, 2018). Close to this side, were confirmed seven mine entrances (Hauptmann, 1980).

Dating of the slag at al-Ṣalaylī is complicated because this locality can include slags from early, middle, and late Islamic production (Yule et al., 2021b). Slag fields (and ancient mines) in general usually have a minimal output of archeologically datable finds (Hauptmann, 2007). Pottery findings are low in those slag fields, but stone finds can occur and be helpful with a rough chronological categorization. Rough dating can also be provided on the basis of exploration and understanding of slag heap surrounding such as settlements and necropolis (Hauptmann, 2007). Based on a field report (Yule et al., 2021b) from al-Ṣalaylī site we know that Early Islamic slags can be identifiable. The middle Islamic period is possibly the main period of mining (Yule et al., 2021b). Slags were recycled in the late Islamic period (Yule et al., 2021b). For the use of mine there is lack of evidence (Yule et al., 2021b). The evidence of EIA mining is indicated by copper slag found in the walls of 6 tombs in al-Ṣalaylī site 1 (Gaudiello and Yule, 2018). Several of EIA hut tomb and Muslim period building contained slag as a fill or building material (Gaudiello and Yule, 2018). Typical early Islamic form and size shows by better preserved slag fragments (Yule et al., 2021b), one furnace slag fragment with the surface smooth on the bottom being the interface between the slag and matte or indeed copper metal that was separated and processed elsewhere on the site (pers. comm. J. Lehner). A rough impression of the furnace sizes can be provided by projected diameter of the furnace slag (Yule et al., 2021b). The appearance of slags can be various, and slags can by dated by different methods. C-dating is a really promising method of dating mines which could be connected with slags, thanks to torches, wood, or charcoals from fire settings left in shafts (Hauptmann, 2007). Slag thus found in the structure of building can be dated and compared with each other in terms of chemical composition and flowing textures (Gaudiello and Yule, 2018). A few smaller areas with slags remain are near to al-Ṣalaylī. 6 km east from al-Ṣalaylī at Bilad al-Ma'din was excavated 74 hut tombs and 43 cylindrical tombs (Yule et al., 2021b). In context with pottery a copper slag could be dated to EIA, but the majority is of Islamic date (Yule et al., 2021b). At the lower end of al-Ṣalaylī *wadi*, 400 m west there lie long abandoned mines used in Muslim times, but probably also used during EIA (Gaudiello and Yule, 2017). Wadi Sa' is a site consisting of ancient tombs and 3 copper production zones, a copper mine and Islamic copper slag and building. The Majazah mine shows undated mining of Cu, Co, and Fe (Yule et al., 2021b).

4. Copper metallurgy

Since there are not many preserved and available samples of ancient raw metals, such as ingots or master alloys, for study, the attention should be drawn to an extensive slag heaps of changing degrees of antiquity existing around the world (Franklin et al., 1976). Before smelting process alone, ores and minerals was usually crushed and grinded (benefication) with hammer stones, which were also used for mining (Weeks, 1997; Weisgerber and Willis, 2000; Garba, 2014). Example of methods of copper sulphide ore reduction that could be used for ancient smelting (**Eq. 1**: Oxidation roasting; **Eq. 2**: Sulphation roasting):

$2CuS + 3O_2 \rightarrow 2CuO + 2SO_2$ (Eq. 1)

$CuS + 2\ O_2 \rightarrow CuSO_4$ (Eq. 2)

According to Jesus (1976) first method (**Eq. 3, 4)** have advantage over second (**Eq. 5, 6, 7)** because it is simpler, but it could cost potential loss of copper. First method: dead roasting of chalcopyrite or another copper sulphide until all the copper ore is oxidized, then copper oxide is smelted in a reducing atmosphere (Jesus, 1976):

$CuFeS_2 + 3O_2 \rightarrow CuO + FeO + 2SO_2$ (Eq. 3)

$2CuO + 2C \rightarrow 2Cu + 2CO_2$ (Eq. 4)

In the first step of second method **(Eq. 5)** the copper ore (chalcopyrite) is roasted till iron sulphide separate from the copper sulphide, which results in copper matte, with copper content about 40–60 %, collecting at bottom of the furnace and slag formed at the top is tapped of (Jesus, 1976). The copper sulphide, still slightly blended with impurities, is after roasting divided by hand from the rest of the gangue and is put through an oxidation phase of process **(Eq. 6)**, then finally the copper oxide is smelted, as beyond, in a reducing atmosphere (**Eq. 7**) (Jesus, 1976):

$2CuFeS_2 + 3O_2 \rightarrow 2CuS + 2FeO + 2SO_2$ (Eq. 5)

$CuS + 2O_2 \rightarrow 2CuO + SO_2$ (Eq. 6)

$2CuO + 2C \rightarrow 2Cu + 2CO_2$ (Eq. 7)

Copper smelting procedure is the main step of primarily copper production by extracting of metallic copper from ores with heating them to a high temperature in furnaces (made of stone or clay) with suitably reduced atmosphere abundant in carbon monoxide (Dungworth, 2012;

Garba, 2014). Copper, usually with impurities (arsenic, sulphur, iron, nickel, silver), and slags are the outcome is (Dungworth, 2012; Garba, 2014). Slag can be using self-fluxing charge (Manasse et al., 2001) or fluxes can be deliberately added to the process. The charge normally contained natural impurities (e.g., CaO), which resulted in the slag calcium olivine is present in abundance (Manasse et al., 2001). Smelting process cast-off supportive technical ceramics such as crucibles, tuyeres, and moulds (Garba, 2014). Casting is a common method when liquid metal is poured into the moulds to create of artefacts with distinct shapes, especially with lost wax technique, and in EIA was usually performed inside of the settlements (Hauptmann, 2007; Garba, 2014). Moulds for casting of copper could be made from stone, clay, copper, or bronze, but with metal moulds were problem of fusing the cast metal to the mould which needed to be mechanically separated (Bamberger et al., 1986). Crucibles were also used either in roasting process to refine copper ore by realising of unwanted oxide malachite to get copper directly by "Crucible smelting" (Moorey, 1999) or in EIA for alloying and casting as a part of secondary copper production (Garba, 2014). Secondary copper production process produces finished copper or copper-alloy artefacts (Dunghworth, 2012; Garba, 2014). Slags were usually recycled, as technology was getting more advanced, in order to get more copper from earlier period slags by crushing with tools as hammers stone, stone anvils and mortars cut into the sandstone and remelting (Hauptmann, 2007).

4.1. Chronology and technology

To understand the dynamics of one particular site and its periods we need to understand the whole complexity of different periods and places generally across Oman. The first plausible chronological scheme and study of the early mining and smelting of the central part of Oman was made by the Bochum team in the early 1980s (Yule, 2021a). Hauptmann (1985) was familiar with al-Ṣalaylī valley slags, but he did not include them into his dating typology, because the examples from another sites represents the chronology better (Yule, 2021a).

The Great Transformation, from hunters and gatherers into farmers and fishermen living clustered into settlements around 200 habitants, was during the 4th millennium BCE. From this period are the first copper object findings and products of cold hammering in Oman (Cleuziou and Tosi 2007; Garba, 2014). The earliest technology originates in the Chalcolithic (ca 4500 – 3600 BCE) period (Hauptmann, 2007), when it was developed (Ben-Yosef et al., 2008). At the beginning of EBA small reaction vessels were used for smelting with the use of crucibles (Hauptmann, 2007). These slags had still remarkably high content of copper (Hauptmann, 2007). Until the EBA II (ca 3000 – 2000 BCE) was common to use pit furnaces into which

copper ore and flux was launched with or without a crucible, this had produced furnace slags (Ben-Yosef et al., 2008). The result of melting was partially smelted ores, which were part of inhomogeneous slag which was usually taken from the furnace and crushed to extract copper (Ben-Yosef et al., 2008). Extensive copper ore mining and smelting, as suggested by the archaeological evidence, starting in the 3rd millennium BCE, and following export (of copper ingots, which was produced primary for export purposes) to the neighbouring regions (Peake, 1928; Gale 1985; Potts 1993, 1999; Hauptmann, 2002; Weeks, 2003b, 2007; Begemann, 2010; Cleziou and Tosi, 2007; Weisgerber 2007). Metal workshops were dedicated to the copper-based production of local artefacts (Weeks, 2003a; Yule, 2014). Copper extraction became the main part and sector of the economy during the 3rd millennium BCE (Cleziou and Tosi, 2007). During the Hafit period (3000 BCE – 2700 BCE) was something like an experimental phase in which various copper-based raw materials, such as malachite or other copper minerals and ores, were randomly added and mixed during the smelting process (Hauptmann et al., 2000). Umm an-Naar period (2700 BCE – 2000 BCE) is characterized by mining, smelting and copper production in large scale (with the percentage of As and Ni) near to the mining sites (Prange, 2001; Weeks, 2003a, 2007; Begemann et al., 2010). In the 2nd millennium BCE were introduced more advanced technological processes such as furnace smelting together with more wide appearance of more durable copper alloys such as tin bronzes and new casting techniques (Begemann 2010; Weeks 1997). Probably the best example of smelting furnaces from LBA and IA are from Timna (Rosenberg, 1980; Hauptmann, 2007). With this knowledge based on finds from Timna was formed a hypothesis that the cylindrical shaft furnace (high 0.5 to1.5 m) was ordinary type of smelting furnace since the end of the 2nd millennium BCE (Hauptmann, 2007). Crushed slags are a typical characterising of the IA smelting site in Israel, they were crushed in order to reprocess and extract more metal from existing slag (Hauptmann, 2007). “Dark age” as was Wadi Sūq Period (2000 BCE – 1350 BCE) labelled, was copper product at least at the same level as during the 3rd millennium BCE (Weeks, 2003a). EIA is in South-eastern Arabia archaeology known as “Lizq period” or “Rumaylah I and II periods” as several Omani sites provide evidence of the recycling and production of copper-alloy based metal objects (Yule, 2014; Giardino and Genchi, 2014). Previous technology was replaced with tapping slag, which is the result of complicated smelting process targeted at achieving completed separation between slag and metallic copper (Ben-Yosef et al., 2008). The heaviest part of the melted mixture drops to the bottom of the furnace and solidifies in the form of a significant copper piece in this technique (Ben-Yosef et al., 2008). The lighter substance was poured out of the installation after it was tapped off. This method evolved through the time and culminated in the

Islamic Period (640 – 1099 CE) with the introduction of slag rings, which were made by pouring the melt in circular depression (Ben-Yosef et al., 2008). Usually tapping slag cools very fast, less than an hour, and furnace slag cools more slowly, but is cool enough to touch in a few hours (Ben-Yosef et al., 2008). Slags generally/usually have a glassy texture, iron oxides and metal phenocrysts (Ben-Yosef et al. 2007) Furnace slag tends to be a smaller amount of glass than tapping slag, but glass can be still observable (Ben-Yosef et al., 2008). Furnace slag can be also cooled quicker if the furnace was broken apart while it was still hot (Ben-Yosef et al. 2008).

4.2. Mineralogy of old metallurgical copper slags

Metallurgical slags are a by-product of smelting activities from the production of metals (Kierczak and Pietranik, 2011; Piatak and Ettler, 2021). Slags are waste products, but also reusable materials, mixtures created during smelting from gangue and fluxes (Hauptmann, 2007; Piatak and Ettler, 2021). This process requires a series of various activities that relate to the physical and chemical transformations of ore into the metal (Hauptmann 2007). The chemical composition of slag can be affected by added fluxes as well as can also contains pieces of clay along with rocks from furnaces or charcoals from wood (Hauptmann 2007; Ben-Yosef 2008). Depending on composition of slag and cooling rates, slags can be crystalline or glass-like and usually rich in silica (Piatak and Ettler, 2021). In general, archaeometallurgical slags consists of very fine grained mixtures of different phases due to rapid cooling from the mineralogical point of view, slags are mainly composed of glass, which as a basic material fills the spaces between the individual grains of the other phases, we also distinguish surface glass, which cools very rapidly without crystallization of the other phases on direct contact with the vessel or crucible into which the slag is melt is discharged (Ettler, 2000; Ben-Yosef 2008). The density of the slag melt is affected by melting temperature and depends on the chemical composition of the source ore and added fluxes which can also affect its appearance, size, mineralogy, and texture (Ben-Yosef, 2008). The porous slag material has a lower viscosity index and is generally less enriched with metals in contrast with massive slags (Bachmann, 1982; Kierczak and Pietranik, 2011). The viscosity of the slag can be increased by added oxides like SiO_2 or Al_2O_3 or decreased by adding CaO (Bachmann, 1982) in ancient metallurgy were usually components of the host rock of the ore itself (Hauptmann, 2007). These fluxing agents can be split into basic, acidic, and neutral (Hauptmann, 2007). Tapping slags are characteristic by free flowing out of the furnace as low viscous, homogeneous part melt with pillow-like structure and cooling rims around each glassy slag-bulges, that can be interpreted as evidence

of temporal periods during the solidification of melt (Hauptmann, 2007). The furnace slag, with common inclusions or imprints of charcoal, is cooled significantly more slowly than tap slag (Hauptmann, 2007).

___Own research of the slags and copper metals

5. Analytical methods

5.1. Samples

The study area with the slag heaps of our interest is located at the al-Ṣalaylī valley of Al-Hajar Mountains in the North Sharqiyah region in the South-eastern Arabia. The area of our interest is concentrated in the vicinity of the randomly taken surface samples from Box 1 (**Fig. 4)**. The studied archaeological site consists of a settlement, burial area, and slag heaps. Cu site al-Ṣalaylī (**Tab. 1**) is 1.36 km away from the nearest highest hill (22.940110, 58.290169) and 21.47 km from Samal Al-Shan Grand Mosque (22.783724, 58.142981). All slag samples (VCS-A, VCS-B, VCS-C, VCS-D; later in text marked only as A, B, C, D) were collected from slag fields (grey colour in **Fig. 3**). The **Tab. 1** gives the coordinates of the access road to the archaeological site designated as "Cu site al-Ṣalaylī ", a “Settlement” also known as Persian village, the "Weathered Cu loc." is a spot with a weathered copper outcrop, the location of the "Primary Cu loc." was once a mining site and samples "F" and "G" were taken in Box 2 "Chrysotile loc." described as host rock (**Fig. 4**).

Table 1: Coordinates from field trip at al-Ṣalaylī site provided by J. Trubač

ID	Latitude	Longitude
Cu site al-Ṣalaylī	22.92851	58.285987
Settlement	22.929209	58.288709
Weathered Cu loc.	22.929777	58.290240
Primary Cu loc.	22.929415	58.290514
Chrysotile loc.	22.926548	58.289585

Four slag samples were collected during the field work in Oman by RNDr. Jakub Trubač Ph.D. Samples were non-professionally, from an archaeological point of view, taken from the surface, so we are missing some stratigraphical and chronological context. The most representative samples were selected for the preparation of thin sections (30 μm). Almost all samples (A, B, C) are tapping slags which resulted from a complicated smelting process in which lighter material was tapped off and allowed to pour out of the furnace installation (Ben-Yosef et al., 2008). This tapping slag cools on the ground and frequently has observable flow textures and can be very glassy. Tapping technology evolved considerably through time culminating in the Islamic Period (Ben-Yosef et al., 2008). Historical slags were generally air-cooled (Kierczak

and Pietranik, 2011). All slag fragments were porous which may be caused by gas leakage during cooling of slag melt.

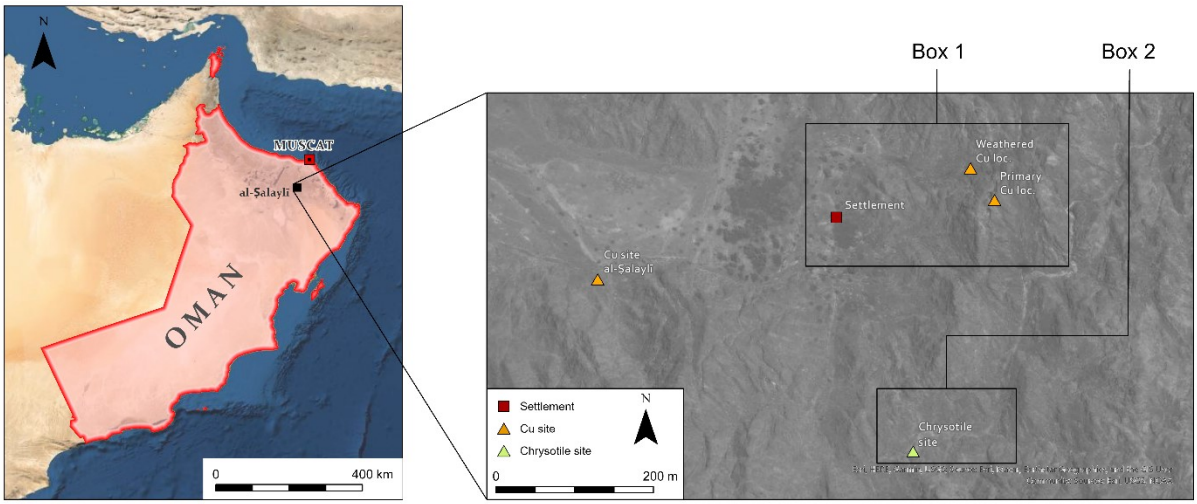

Figure 4: Locality of al-Ṣalaylī in Oman and coordinates from ***Tab. 1,*** *with boxes with area of collected samples*

Tapping slag A (**Fig. 5**) with a distinct flow texture corresponds to historical copper slags produced from BA, but also as Paul Yule mentioned, it can be from LIA to the middle Islamic period. It was found as a 13 cm fragment of massive and heavy material of dark grey and brown colour, in a small area partly with a weathered green surface. Remelting of this material is unlikely due to the higher copper content, so it is assumed that slag is from the primary production of copper. There is a hole vertically through the slag as you can see at the picture and numerous relatively large vesicles.

Figure 5: Photograph of slag A; Author: Pavel Škácha

Tapping slag B (**Fig. 6**) is very similar to slag A with less visible flow texture with pores. The green weathered surface cover is present. The estimated age is the same as for the other samples due to their similar appearance.

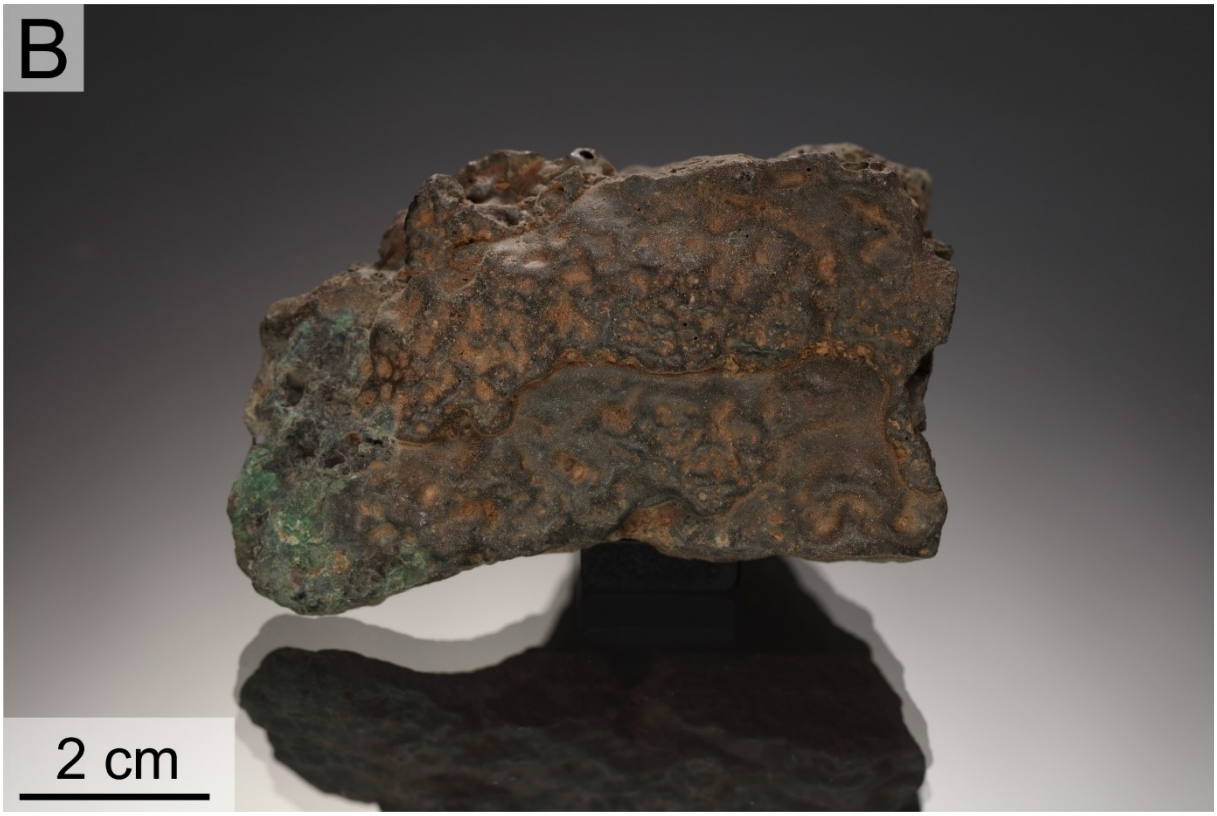

Figure 6: Photograph of slag B; Author: Pavel Škácha

Tapping slag C (**Fig. 7**) has a pillow-like surface with visible bubbles. The sample is markedly heavier and larger than previous samples. The colour is dark grey to reddish brown, unlike samples A and B the surface is minimally weathered. The flow texture is also noticeable along with inclusions of clay or reddish dirt. At bottom right part of picture can be seen inclusion with more porous vesicular texture.

Figure 7: Photograph of slag C; Author: Pavel Škácha

Slag D (**Fig. 8**) was different from previous slags, which can indicate either a different type of slag (furnace slag), or a different period when it was manufactured. The surface of slag was weathered. In the slag D, during the process of making a thin section was found embedded charcoal fragments. This slag had the potential for independent dating without relying on an archaeological context, which is missing. After a thin section was made the cut slag inside showed visible copper, the freshly cut surface reacted with the air as could be observed under the microscope.

Figure 8: Photograph of slag D; Author: Pavel Škácha

5.2. Performed analyses

In the laboratories of the geological institutes at the Faculty of Science, Charles University (Ing. Věra Vonásková, Lenka Jílková), were obtained several data, including the bulk chemical composition of slags, trace element analysis and silicate analysis, the bulk chemistry of slags was determined using methods adapted to slag materials. Analysis of the solutions was performed using an inductively coupled plasma optical emission spectrometer (ICP- OES; Agilent 5110, USA) and an inductively coupled plasma mass spectrometer (Thermo Scientific™ iCAP™ SQ ICP-MS, Germany). Total carbon (C_{tot}), inorganic carbon (C_{inorg}) and total sulphur (S_{tot}) were determined using a combination of Thermo Scientific™ iCAP™ SQ ICP-MS (iCAP™, Germany).

The X-ray diffraction analyses (XRD) of the samples were performed using a PANalytical X`Pert Pro diffractometer equipped with a diffracted-beam monochromator and X`Celerator multichannel detector. The analysis conditions were as follows: CuKa radiation, 40 kV, 30 mA, step scanning at 0.02°/100 s in the range 3–80° 2q. The qualitative analysis employed the X`Pert HighScore software 1.0d, equipped with the JCPDS PDF-2 database (ICDD, 2002). ICDD, 2002. JCPDS PDF-2 database. Newton Square, PA, USA.

The slags A, B, C, and D were selected as representative samples for a detailed study using the optical and electron microscopy. Polished thin sections (**Fig. 20**) of selected samples were analysed at the laboratories of the Institute of Petrology and Structural Geology at the Faculty of Science, Charles University in Prague. For the investigations of samples was used a JEOL JXA-8530F electron probe micro-analyser (EPMA) is equipped with five wavelength-dispersive spectrometers. The installed detectors for secondary electrons and back-scattered electrons (BSE) were used for imaging. The quantitative chemical spot analyses were acquired by using the associated wavelength dispersive spectrometers under the backscattered electron (BSE) images and quantitative microanalyses were acquired with the electron probe microanalyser JXA-8530F at the Institute of Petrology and Structural Geology (Charles University, Prague). Quantitative analyses were acquired with accelerating voltage 15 kV, 15 nA beam current, and 30/15 s counting time for peak/background. Following standards were used for the quantification of analysed elements: Si—quartz, Al—corundum, Ti— rutile, Cr—chromium oxide, Fe—magnetite, Mg— periclase, Mn—rhodonite, Ca—diopside, Na—albite, K—sanidine, P— apatite, Cl-tugtupite, S-celestite, V-vanadium, Ba-baryte, Zn-sphalerite, Ni-nickel, and Cu-cuprite. Kα lines of the characteristic X-rays were used for the detection of all the elements except for Ba (Lα). ZAF procedure was applied for the correction of the matrix effects. Following diffracting crystals were used for the detection of the characteristic X-rays of analysed elements: TAP (Si, Al, Mg, Na, P), PET (Ti, V, Cr, Ca, K, Cl, S, Ba), and LIF (Fe, Mn, Zn, Ni, Cu). Detection limits are in supplements (**Tab. 8)**.

Abbreviations of mineral phases are used based on Warr (2021).

6. Results

6.1. Bulk geochemistry of slags

The chemical composition of the slag samples is reported in **Tab. 2**. In the overall chemical composition of the studied slags, iron oxides/divalent iron have the highest representation (30.7 to 39.4 wt.% FeO), followed by silicon (28.7 to 38.2 wt.% SiO_2) and trivalent iron oxide (7.40 to 8.56 wt.% Fe_2O_3). Elevated concentrations of Mg and Ca are probably pointing on the used material of magmatic mafic rock. On the contrary, the alkali content and aluminium content is low (0.25 to 0.36 wt.% Na_2O and 0.47 to 0.58 wt.% K_2O and 1.34 to 1.76 wt.% Al_2O_3). Small amounts of CO_2, S, TiO_2 and P_2O_5 were also detected (**Tab. 2**).

In order to predict the basicity of slags and thus also their phase composition, the viscosity index (v. i.) according to Bachmann (1982), measuring the ratio of “basic” (CaO, MgO, FeO,

MnO, Na_2O, K_2O) to “acidic” (SiO_2, Al_2O_3) oxides, was calculated (Kierczak and Pietranik 2011). The viscosity index (v. i.) of the slag samples is relatively high, marking the basic composition and meaning that slag melt had lower viscosity **(Eq. 8)**.

$$v.\ i.=(\sum CaO+MgO+FeO+MnO+Alk_2O)/(\sum SiO_2+Al_2O_3) \quad \text{(Eq. 8)}$$

In all samples, the copper content was significantly elevated, reaching the highest amount of 26050 mg/kg in sample A, slightly lower in sample B (23340 mg/kg) and the lowest content was measured from sample C (3920 mg/kg). Higher contents of several other heavy metals + strontium was also measured (Co 244–602; Cr 1970–2220; Ni 66.5–228; Sr 481–630; Zn 325–395 mg/kg; **Tab. 2**).

Table 2: The results of the silicate analysis and the analysis of the trace elements of the slags from al-Ṣalaylī

Sample (wt.%)	A	B	C
SiO_2	28.7	33.7	38.2
TiO_2	0.05	0.09	0.06
Al_2O_3	1.34	1.76	1.56
Fe_2O_3	8.36	7.40	8.56
FeO	39.4	35.5	30.7
MnO	0.04	0.05	0.06
MgO	4.92	5.54	5.23
CaO	9.20	8.72	11.70
$N_{a2}O$	0.25	0.36	0.28
K_2O	0.47	0.63	0.58
P_2O_5	0.09	0.06	0.11
H_2O^-	0.03	0.11	0.13
H_2O^+	0.39	0.01	1.14
CO_2	0.30	0.17	0.13
S	1.43	1.71	0.62
Total	94.92	95.74	99.05
Sample mg/kg	A	B	C
Ag	<5	<5	<5
As	<25	<25	<25
Ba	30	41	46
Bi	<25	<25	<25
Cd	<2	<2	<2
Co	602	584	244
Cr	1990	2220	1970
Cu	26050	23340	3920
Ga	31.5	30	27
Ge	<5	<5	<5
Mo	<5	<5	<5
Ni	228	183	66.5
Pb	<15	<15	<15
Sb	<15	24.5	19.5
Se	<40	<40	<40
Sn	<15	<15	<15
Sr	481	527	630
Zn	325	395	343
v. i.	1.81	1.43	1.22

6.2. The phase composition of slags

From almost all the samples that were provided from the Omani field trip by J. Trubač were performed X-ray powder diffraction analyses. In **Fig. 9** you can see the record of the selected four slags (A, B, C, D).

From the slag sample A were used two samples: two macroscopically different parts for the phase composition analysis, less weathered labelled as A, taken from the core of the sample, and more weathered A1 from the green weathered surface of the slag A. The mineral composition of A was analysed to fayalite, ankerite, bornite, quartz and monticellite. The sample A1 consist of monticellite, quartz, magnetite, brochantite.

Slag B shows the composition of magnesian fayalite, clinopyroxene (diopside) and monticellite.

Minerals detected in slag C consist of augite, fayalite (Mg, Mn), lizardite, and low chalcocite.

Slag D, as was mentioned earlier, is composed of a large proportion of copper, as could be recognised macroscopically. The X-ray diffraction also confirmed dominant copper and recognized also phases as cuprite, hematite, tenorite, quartz, lizardite, and iron.

The sample E is described as a weathered zone and composed of goethite, clinochlore, lepidocrocite, quartz, and hematite.

Specimen F was recognised as a friable chrysotile ophiolite and consists of dolomite, spangolite, chrysotile, lizardite, diopside, and calcite (Mg). Sample F1 from the same container as F is described as host rock and compact containing antigorite, lizardite, calcite, olivine, and enstatite. Sulfidic specimen G with yellowish colour showed only lizardite. This samples were collected at Chrysotile loc. as you can see in **Tab. 1**.

The H samples were recognized as copper alterations, separated to H1, H2 and H3. The $H1_{Cu}$ bears antigorite, lizardite, and brochantite; in $H2_{Cu}$ were found brochantite and lizardite; $H3_X$ with a black surface, possibly from Mn-oxides, showed the presence of lizardite, magnetite, clinochrysotile, sodalite, brochantite, and quartz. $H3_{Cu}$ in XRF showed just brochantite and lizardite. In a few more samples the presence of sodalite was also recognized.

The JT samples are represented just as small fractions of formerly larger samples and the RXF analysis showed on brochantite composition.

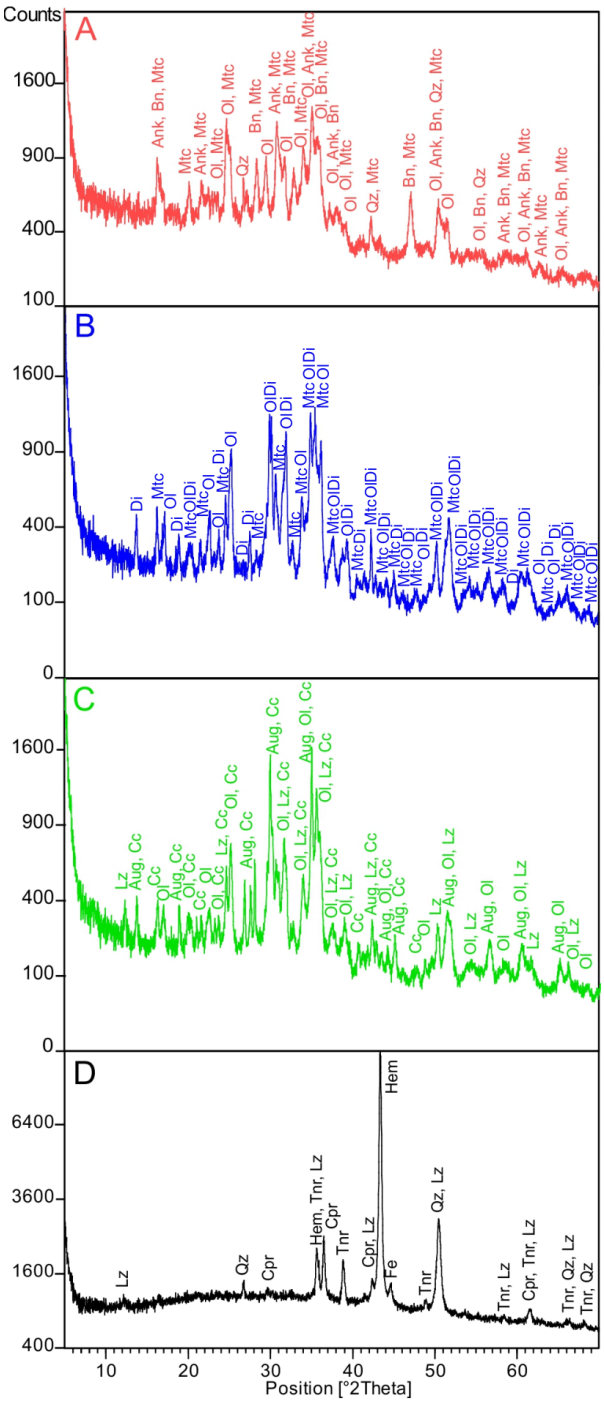

Figure 9: Diffractograms from analysis of slags A - red, B - blue, C – green, D – black

6.3. Petrography

The studied slags demonstrate slightly different mineralogical compositions in all samples as expressed on XRD patterns below. The mineral assemblage of the A, B, and C is dominated by Fe-olivine (fayalite), showing mostly euhedral prismatic to skeletal crystals of varying size, euhedral clinopyroxene crystals of skeletal or elongated dendritic shape, and residual glass

matrix (**Fig. 10**). Among the minor phases are commonly present small, rounded crystals of spinel and scattered copper. Small amounts of various Fe- and Mg-oxides or Fe- and Cu-sulphides are also present. The D samples dominates a large portion of copper, but a minor amount of olivine, pyroxene, Fe- and Mg-oxides and Fe- and Cu-sulphides is observable. In all samples are present rounded holes in thin sections, previously gas vesicles. Common are also chilled margins reflecting faster cooling resulting in smaller crystals and more glass matrix on the surface of the former slag melt.

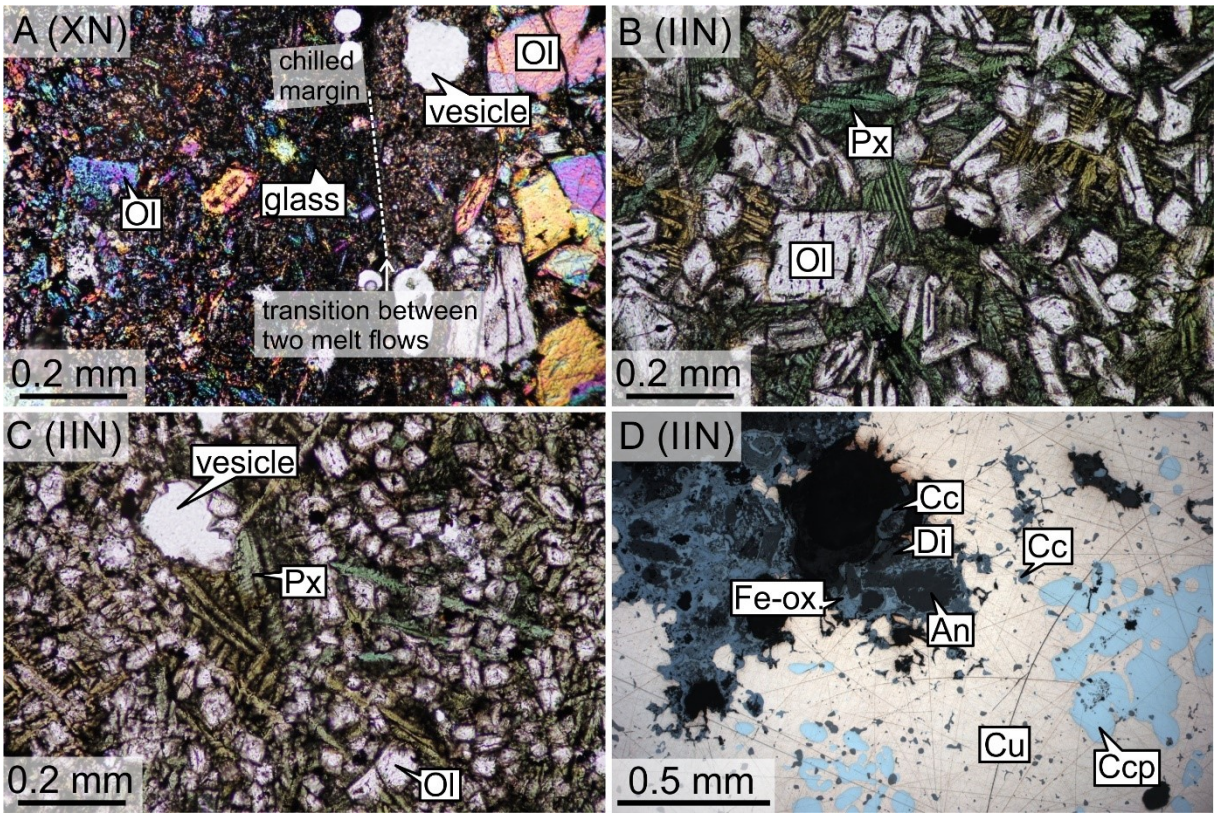

Figure 10: thin sections of slags (IIN -plain polarised light; XN-crossed nicols); A (XN): t wo interlocking slags separated by a cooled rim, on the left with a predominance of forsterite and on the right with a predominance of fayalite with a visible white spots=vesicles, glass matrix; B (IIN): euhedral to subhedral prismatic olivine crystals surrounded by skeletal to dendritic green to brown clinopyroxene; C (IIN): euhedral to subhedral olivine and elongated clinopyroxene crystals; D (IIN): iron oxides probably magnetite, Cc (chalcocite), An (anorthite), Di (diopside), Ccp (chalcopyrite)

In the slag A **(Fig. 10A, 11A)** are dominantly present euhedral to subhedral crystals of olivine of various sizes. Fayalite and forsterite are occurring. Large phenocrysts of olivine (⌀ ~ 0.1–0.2 mm) with prismatic or slightly skeletal and less often tabular shape are surrounded by smaller olivine and clinopyroxene crystals in a glass matrix. The fine-grained matrix can be found as a part of the chilled margin neighboured by the coarse-grained part. Clinopyroxenes are present as euhedral dendritic or occasionally columnar crystals of small size (⌀ ~ 0.01 mm). Small rounded euhedral crystals of spinel rich in chrome are common in the matrix or as inclusions in olivine phenocrysts. And it also contains many small grains of copper, and copper droplets.

Exsolutions visible at **Fig. 11** show mixing of bornite and copper sulphides (Cu_3S_2) and enclosed copper grains with iron oxides rim.

The slag B (**Fig. 10B, 11B)** can be texturally separated into the two parts, one with coarser grains of olivine (Mg-fayalite to Mg-forsterite) which gradually passes into a fine-grained second part with the presence of chilled margins, where the crystals grew faster but smaller due to faster cooling of the melt. Crystals of olivine (edges of monticellite), which is the main phase which has chain habitus with H-shaped cross-section to grid-like and small feather-like crystals and show commonly chemically zoned phenocrysts. Large olivine crystals enclose small, rounded spinel grains and "pure" copper droplets. This slag has numerous vesicles (bubbles). Olivine phenocrysts are markedly dominant in size in one half of this thin section, but gradually decrease in size and clinopyroxene begins to predominate. Compared to slag A, this slag B has a very high content of green crystals of clinopyroxene which are dendritic to elongated skeletal or even feather-like textures. By spot analysis on a microprobe were also found chalcopyrite, pyrrhotine, chromite, and bornite.

Slag C (**Fig. 10C, 12C**) has different sizes of olivine crystals which either transition smoothly or there are observable jumps in crystal size, the space between the olivine is occupied by clinopyroxene more abundantly than in previous thin sections (A, B). The main phase in this sample is pyroxene, which is light green to brown with elongated skeletal crystals under optical microscope. Olivine has small euhedral to subhedral crystal which are slightly porphyry or prismatic. Commonly are also present rounded vesicles, previously containing gas. The structure of the thin section is changing near to edges where there is present small quartz and calcite chunk. Accessories of a small crystal of spinel, bornite and chromite are common.

Sample D (**Fig. 10D, 12D**) is quite different from slags A, B and C. It is largely composed of copper, copper sulphides, iron oxides and olivine, quartz, and silicates, anorthite, albite, diopside and even a small grain of silver has been found in it. Minor and accessory phases such as amphibole, chalcopyrite, chalcocite, chrysotile, and spinel were also observed. The silicate melt formation contained quartz and pieces of quartz crystals, ashes, glass with bubbles, and alkali. The whole specimen is porous and full of vesicles with crumbled edges where the copper plunges into the olivine. Olivine crystals crystallised skeletally, were elongated, and visibly zoned.

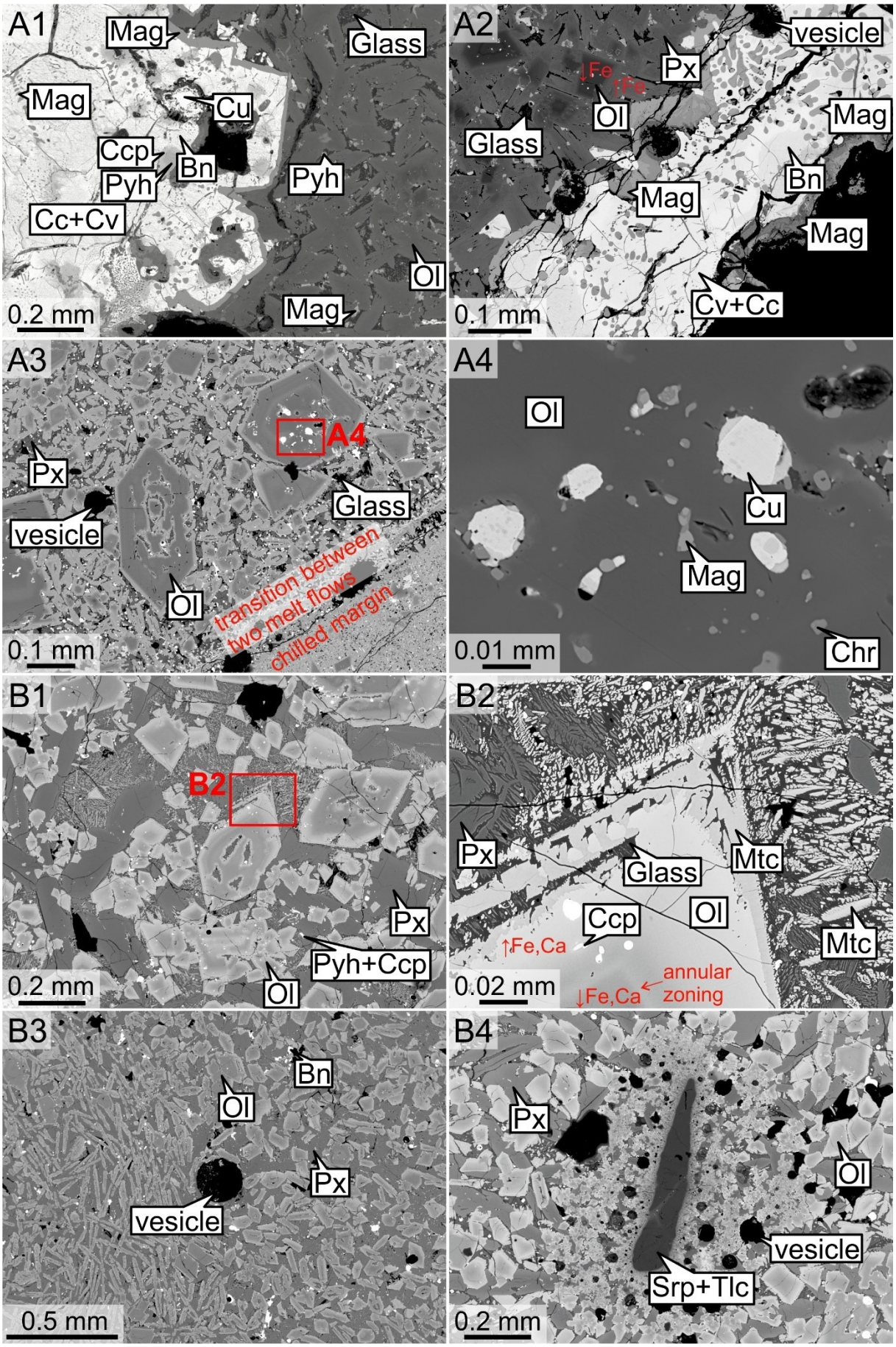
A1
Mag
Glass
Mag
Cu
Ccp
Bn
Pyh
Pyh
Cc+Cv
Ol
Mag
0.2 mm
A2
vesicle
↓Fe ↑Fe
Px
Ol
Mag
Glass
Bn
Mag
Mag
Cv+Cc
0.1 mm
A3
A4
Px
Glass
vesicle
Ol
transition between two melt flows
chilled margin
0.1 mm
A4
Ol
Cu
Mag
0.01 mm
Chr
B1
B2
Px
Pyh+Ccp
Ol
0.2 mm
B2
Px
Glass
Mtc
Ccp
Ol
↑Fe,Ca
Mtc
0.02 mm
↓Fe,Ca
annular zoning
B3
Bn
Ol
Px
vesicle
0.5 mm
B4
Px
Ol
vesicle
Srp+Tlc
0.2 mm

Figure 11: A1: fayalite olivine (40% forsterite) with glassy matrix separated with iron oxides rim from copper sulphides and bornite with pyrrhotine, chalcopyrite and copper grain; A2: olivine and clinopyroxene crystals in glassy matrix separated with iron oxide rim from copper sulphides (covellite and chalcocite); A3:olivines in glassy matrix; A4: grain of copper with As and Ni content, chromite and iron oxide inside of olivine crystal; B1: olivine crystals surrounded by clinopyroxene with small pyrrhotine and chalcopyrite grains; B2: visible monticellite rim of zoned olivine crystal with visible changing content of Fe and Ca, glassy matrix and chalcopyrite; B3: vesicle in middle surrounded by olivine and clinopyroxene crystals, small bornite grains; B4: serpentine phases + talc grain in the middle, possibly from protolith rock, visible replacing of protolith phases by olivine and clinopyroxene crystals with decreasing grain size toward the border with serpentine + talc, common vesicles around

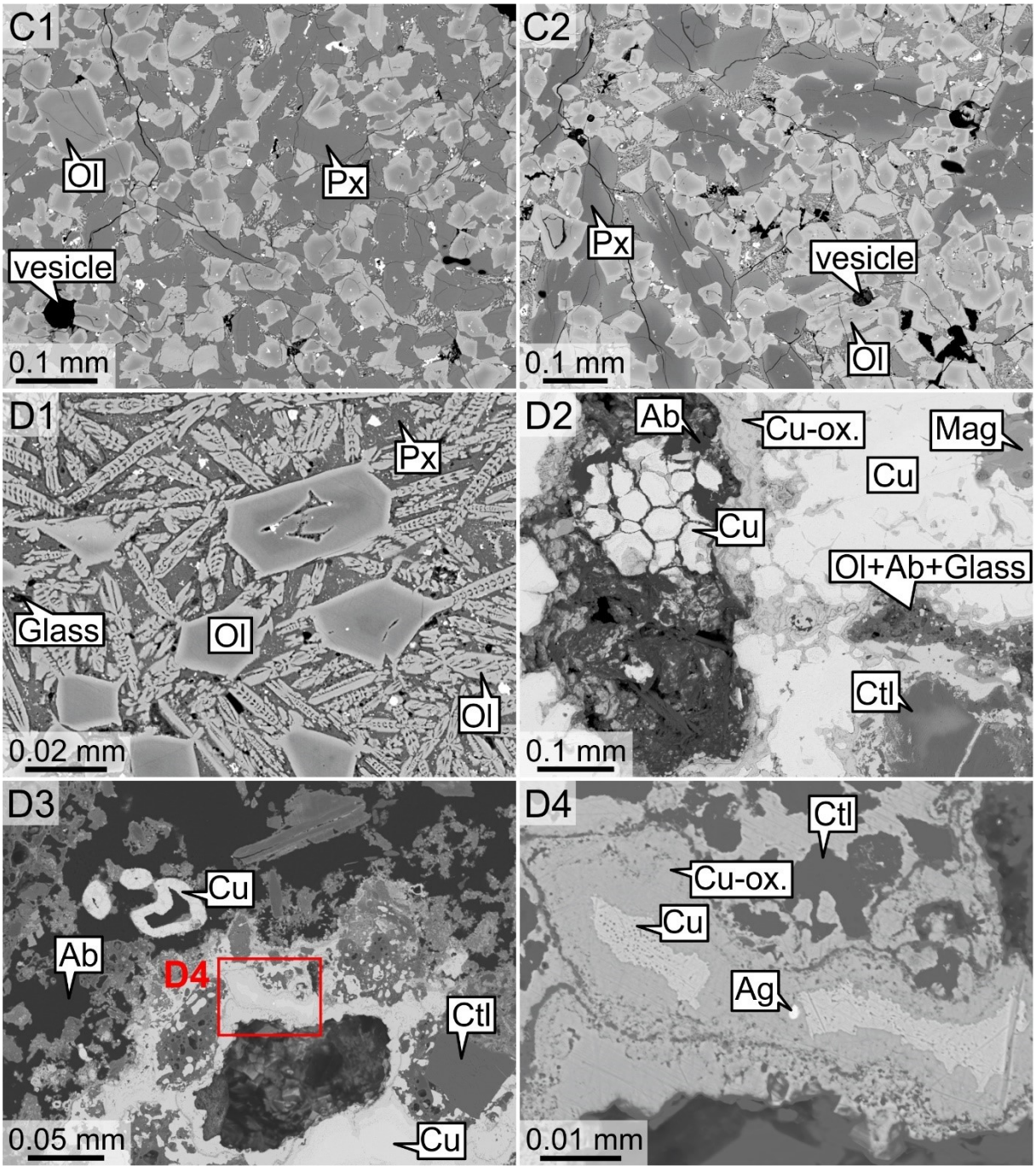

Figure 12: C1 monticellite edges of olivine crystals, clinopyroxene in glassy matrix, vesicle; C2: olivine and pyroxene crystals, vesicle; D1: elongated skeletal olivine zoned crystals surrounded by pyroxene and glass; D2: Copper surrounded by albite, iron and copper oxides with silicates, chrysotile, glass, olivine, albite; D3: Quartz, albite , chrysotile; D4: piece of copper on border small grain of silver enclosed in copper, silicates of glass, quartz

6.4. Mineral chemistry

6.4.1. Olivine

One of the most common silicates observed in the studied slag samples is olivine, which is the most common crystalline phase in the slags (Pearce et al., 2021). Its chemical composition is defined by the solid solution forsterite-fayalite (Mg_2SiO_4–Fe_2SiO_4) (Kierczak and Pietranik, 2011). According to the cooling rate, olivine forms well constrained porphyritic to chain-like crystals with rims in the slags. The growth zoning is frequently shown by olivines, which is a non-equilibrium feature typical of solid solution crystals evolving under fluctuating temperature conditions (Addis et al., 2016). The flexible morphology of olivine crystals in slag can indicate different cooling ways of numerous samples from almost instant to long period of several hours before complete crystallisation (Kierczak and Pietranik, 2011; Ettler et al., 2009b) similarly to volcanic rocks. The crystallisation temperature of olivine can be significantly shifted by occurrence of other chemical components such as Ca, Al and Si which may decrease the crystallisation temperature of fayalite-rich olivine by up to 100 °C, but for example presence of trivalent iron which is indicated by the occurrence of magnetite in the slag, does not significant affect the calculated temperatures (Morton and Wingrove, 1969, 1972). Olivine crystals are zonal, their content of iron and calcium varies, and the rings of increase are affected by temperature. Around big crystals are small skeletal crystals with higher content of Ca. As it can be seen in the ternary diagram below (**Fig. 13**) most of the measured grains of olivine were fayalite, and the Fe-Mg is composition is ranging between 50-90% Fa, at the close 50% border with forsterite end member in hortonolite group. The ratio of X_{Mg} from 0.01 to 0.44, Ca a.p.f.u. (atoms per formula unit) from 0.05 to 0.78, which are closer to the composition of kirschteinite (by RTG recognised as monticellites).

Table 3: Chosen microprobe analysis of olivine of slags from al-Ṣalaylī, Oman (wt.%; BD-bellow detection)

Sample	A	A	A	B	B	B	C	C	C	D	D
Num.	1	3	6	38	39	44	46	54	55	58	59
SiO_2	34.032	31.635	30.150	33.404	30.755	31.442	34.138	31.541	31.653	33.670	31.212
TiO_2	BD	BD	BD	BD	BD	BD	BD	BD	BD	BD	BD
Al_2O_3	0.023	BD	0.198	BD	BD	BD	BD	BD	BD	BD	0.043
MgO	18.80	2.80	0.28	18.54	6.07	0.98	19.01	6.86	1.20	16.46	6.67
FeO	43.01	44.71	53.90	44.38	57.23	43.43	43.72	57.09	45.37	46.81	56.67
MnO	0.034	0.034	0.050	0.023	0.075	0.087	0.076	0.105	0.069	0.069	0.048
CaO	2.75	19.48	13.13	1.42	3.89	22.96	1.76	3.70	21.33	1.70	3.60
Cr_2O_3	0.114	0.116	BD	0.190	0.047	BD	0.224	0.054	BD	0.164	0.311
V_2O_3	BD	BD	BD	BD	BD	BD	BD	0.028	0.032	BD	0.030
ZnO	0.057	BD	BD	BD	0.117	0.071	BD	0.053	0.053	0.077	0.097
NiO	0.030	BD	BD	0.035	BD	BD	0.030	BD	BD	0.048	BD
CuO	0.033	BD	BD	BD	0.041	0.030	0.047	0.073	0.043	0.054	0.078
BaO	BD	0.040	BD	BD	BD	BD	BD	BD	BD	BD	BD
Na_2O	0.051	BD	0.039	0.017	0.028	0.079	0.039	0.011	0.024	BD	BD
K_2O	0.015	BD	0.046	BD	0.020	0.097	BD	BD	BD	BD	BD
P_2O_5	0.072	0.156	0.197	0.040	0.099	0.429	BD	0.056	0.145	BD	0.112
SO_3	BD	BD	BD	BD	BD	BD	BD	BD	BD	BD	BD
Cl^-	BD	0.013	BD	BD	BD	0.010	BD	BD	0.013	BD	0.013
Total	99.09	99.03	98.06	98.10	98.43	99.67	99.12	99.62	100.06	99.10	98.92
O	4	4	4	4	4	4	4	4	4	4	4
Si	1.004	1.002	0.998	1.001	0.999	0.994	1.007	1.006	1.000	1.010	1.002
Ti	BD	BD	BD	BD	BD	BD	BD	BD	BD	BD	BD
Al	0.001	BD	0.008	BD	BD	BD	BD	BD	BD	BD	0.002
Mg	0.827	0.132	0.014	0.828	0.294	0.046	0.836	0.326	0.056	0.736	0.319
Fe^{2+}	1.06	1.18	1.49	1.11	1.55	1.15	1.08	1.52	1.20	1.17	1.52
Mn	0.001	0.001	0.001	0.001	0.002	0.002	0.002	0.003	0.002	0.002	0.001
Ca	0.087	0.661	0.466	0.045	0.135	0.778	0.056	0.126	0.722	0.055	0.124
Cr	0.003	0.003	BD	0.004	0.001	BD	0.005	0.001	BD	0.004	0.008
V	BD	BD	BD	BD	BD	BD	BD	0.001	0.001	BD	0.001
Zn	0.001	BD	BD	BD	0.003	0.002	BD	0.001	0.001	0.002	0.002
Ni	0.001	BD	BD	0.001	BD	BD	0.001	BD	BD	0.001	BD
Cu	0.001	BD	BD	BD	0.001	0.001	0.001	0.002	0.001	0.001	0.002
Ba	BD	0.000	BD	BD	BD	BD	BD	BD	BD	BD	BD
Na	0.003	BD	0.002	0.001	0.002	0.005	0.002	0.001	0.001	BD	BD
K	0.001	BD	0.002	BD	0.001	0.004	BD	BD	BD	BD	BD
P	0.002	0.004	0.006	0.001	0.003	0.011	BD	0.002	0.004	BD	0.003
S	BD	BD	BD	BD	BD	BD	BD	BD	BD	BD	BD
Cl^-	BD	0.001	BD	BD	BD	0.001	BD	BD	0.001	BD	0.001
Total	2.99	2.99	2.99	2.99	2.99	2.99	2.99	2.99	2.99	2.99	2.99
X_{Mg}	0.438	0.100	0.009	0.427	0.159	0.039	0.437	0.177	0.045	0.385	0.173

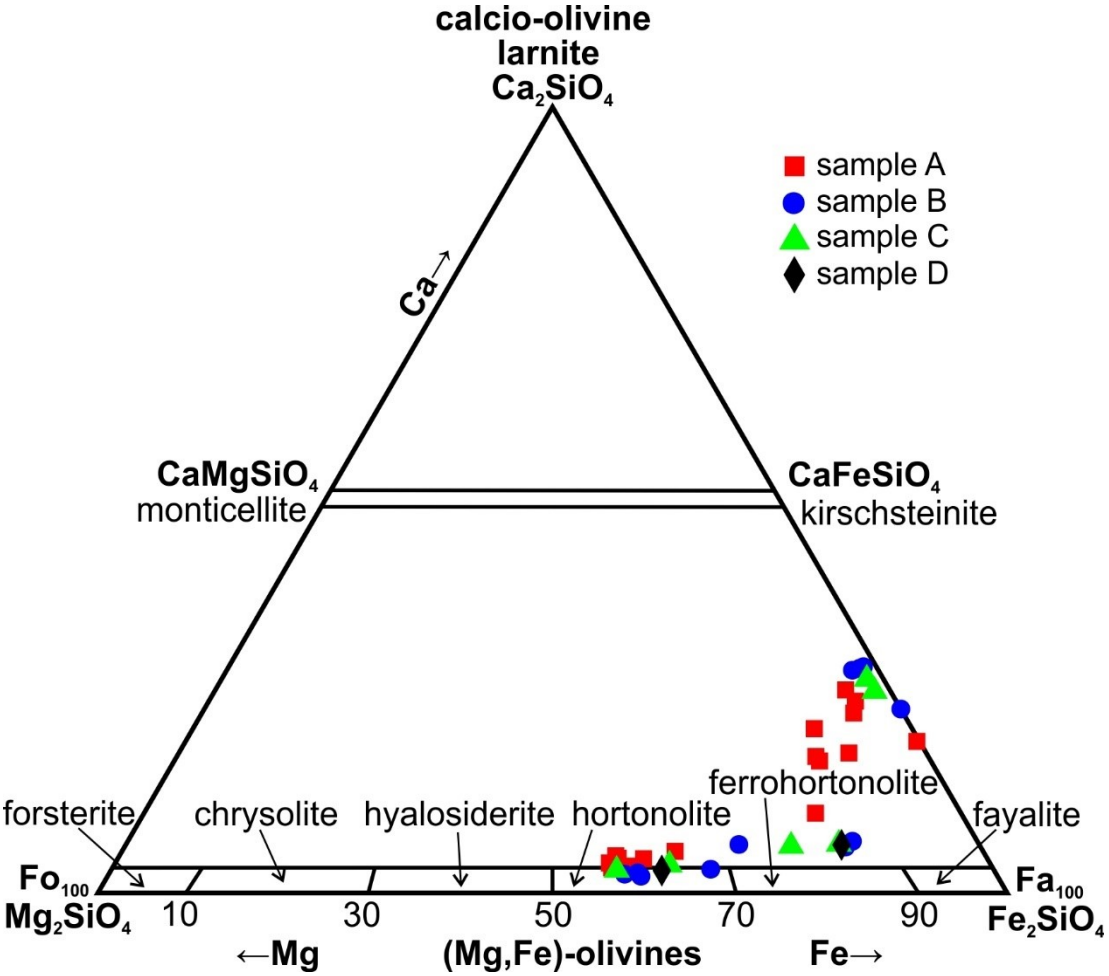

Figure 13: Ternary diagram of olivine and Fe, Ca, Mg members; slag A -red; slag B - green, slag C – blue, slag D - black

6.4.2. Clinopyroxene

Clinopyroxene in slags fills the spaces between olivine and forms a complement to the glassy matrix. The major components in slags being SiO_2, CaO and Al_2O_3 (Pfeiffer, 2012). Clinopyroxene crystals are euhedral to subhedral dendritic even feather-like looking observed in all thin sections. In slag C was pyroxene possibly main phase. X-ray diffractions were used to characterise the phases in the slag. The most common pyroxene, as we can see in the ternary diagram **(Fig. 15)** was augite, with higher content of Fe and Ca. The ratio $X_{Mg} = Mg/(Mg+Fe^{2+})$, is ranging from 0.06 to 0.12.

Table 4: Microprobe analysis of clinopyroxene in slags from al-Ṣalaylī, Oman (wt.%; BD, Below the detection limit; recalculated for 6 O of a.p.f.u.)

Sample	A	A	A	B	B	B	C	C	C
Num.	19	20	21	36	37	43	49	56	57
SiO_2	43.78	43.99	46.28	46.26	46.36	46.24	48.45	50.29	48.24
TiO_2	0.108	0.091	0.112	0.213	0.240	0.198	0.129	BD	0.098
Al_2O_3	3.89	3.64	3.10	3.32	3.32	3.53	1.73	1.05	1.92
MgO	0.96	0.99	1.67	2.12	1.92	1.02	2.83	6.17	2.24
FeO	29.30	29.84	26.97	25.61	25.59	26.74	24.47	19.89	25.66
MnO	0.034	0.042	0.032	BD	0.036	0.030	0.054	0.022	0.019
CaO	20.97	21.08	21.81	21.79	21.83	21.88	21.91	22.25	22.08
Cr_2O_3	0.164	0.109	0.116	0.085	0.071	BD	0.161	0.452	0.182
V_2O_3	0.039	BD	0.058	0.058	0.042	BD	BD	0.048	0.055
ZnO	BD	BD	BD	BD	0.031	BD	0.036	BD	BD
NiO	BD	BD	BD	BD	0.045	BD	BD	BD	0.026
CuO	BD	BD	BD	0.044	0.048	BD	BD	0.040	0.042
BaO	BD	BD	BD	BD	0.062	BD	BD	BD	BD
Na_2O	0.140	0.146	0.205	0.146	0.150	0.153	0.086	0.060	0.098
K_2O	0.015	BD	0.012	BD	0.016	0.024	BD	BD	BD
P_2O_5	0.304	0.298	0.104	0.193	0.103	0.164	0.050	0.101	0.102
SO_3	BD	BD	BD	BD	BD	BD	BD	BD	BD
Cl^-	BD	BD	BD	BD	0.008	BD	0.017	BD	0.010
Total	99.78	100.25	100.49	99.87	99.90	100.07	99.99	100.24	100.80
Si	1.82	1.83	1.89	1.88	1.89	1.89	1.95	1.97	1.94
Ti	0.003	0.003	0.003	0.007	0.007	0.006	0.004	BD	0.003
Al	0.191	0.178	0.149	0.159	0.159	0.170	0.082	0.049	0.091
Mg	0.060	0.061	0.102	0.129	0.117	0.062	0.170	0.361	0.134
Fe^{2+}	1.02	1.04	0.919	0.871	0.871	0.913	0.825	0.650	0.863
Mn	0.001	0.001	0.001	BD	0.001	0.001	0.002	0.001	0.001
Ca	0.935	0.937	0.951	0.950	0.952	0.957	0.946	0.936	0.951
Cr	0.005	0.004	0.004	0.003	0.002	BD	0.005	0.014	0.006
V	0.001	BD	0.002	0.002	0.001	BD	BD	0.001	0.002
Zn	BD	BD	BD	BD	0.001	BD	0.001	BD	BD
Ni	BD	BD	BD	BD	0.001	BD	BD	BD	0.001
Cu	BD	BD	BD	0.001	0.001	BD	BD	0.001	0.001
Ba	BD	BD	BD	BD	0.001	BD	BD	BD	BD
Na	0.011	0.012	0.016	0.012	0.012	0.012	0.007	0.005	0.008
K	0.001	BD	0.001	BD	0.001	0.001	BD	BD	BD
P	0.011	0.010	0.004	0.007	0.004	0.006	0.002	0.003	0.003
S	BD	BD	BD	BD	BD	BD	BD	BD	BD
Cl^-	BD	BD	BD	BD	0.001	BD	0.001	BD	0.001
Total	4.06	4.07	4.04	4.02	4.02	4.02	4.00	3.99	4.01
X_{Mg}	0.055	0.056	0.100	0.129	0.118	0.063	0.171	0.357	0.135

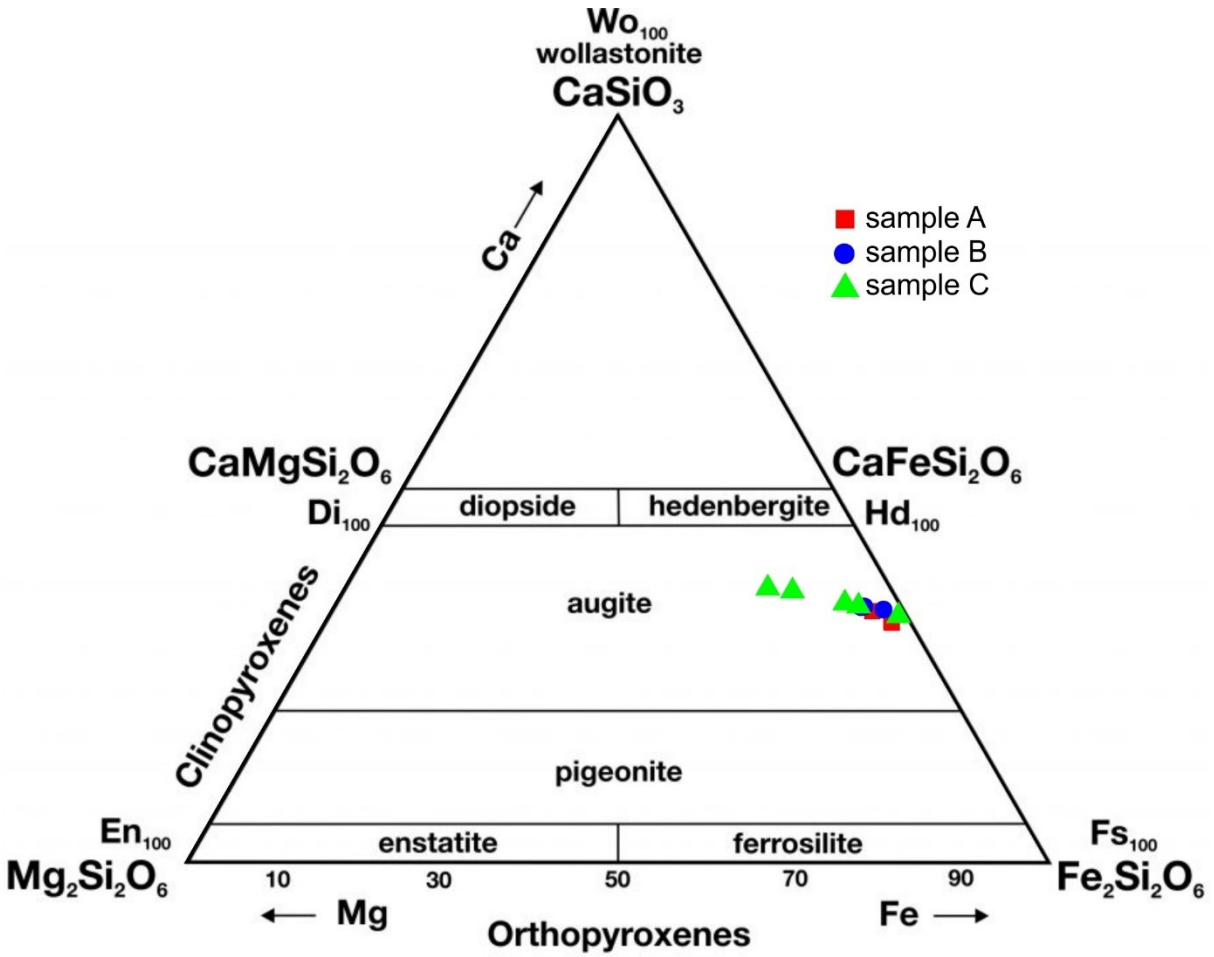

Figure 14: Ternary diagram of pyroxenes and Fe, Ca, Mg members; slag A -red; slag B - green, slag C – blue (Modified after Morimoto, 1989)

6.4.3. Glass

Glass is the most common and typical phase found in metallurgical slags (Ettler et al., 2015). The glass silicate phase was observed in all four examined materials. The glassy matrix is appearing as isotropic and amorphic without pleochroism. It occurs frequently, but in thin residues, so it was difficult to measure on the microprobe. The composition of glass in this type of material is very varied. The glass chemical composition is dominated by SiO_2 (on average 47.53-52.96 wt.%), following FeO (13.96-19.07 wt.%), Al_2O_3 (12.36-15.82 wt.%) and CaO (2.31-6.05 wt.%). If studied materials consist mainly of glass and do not include clinopyroxene crystallites that is believed to be an indicator for relatively slow cooling of the silicate melt (Ettler et al., 2009a), but in this case there is clinopyroxene present. Glassy matrix have a higher content of Si in slag B. Presence of the quartz in slags may be either a sign of unmelted parts of a given charge, unmelted relics of host rock and quartz inclusions as restites (Hauptmann 2000, 2020), or as a silica flux to aid the smelting process (D'Amico et al., 1998)

Table 5: EMPA analysis of glass from slags from al-Ṣalaylī (wt.%), (BD – Below detection limit)

Sample	A	B	C
Num.	13	33	52
SiO_2	47.53	52.96	49.99
TiO_2	0.10	0.28	0.26
Al_2O_3	15.82	13.79	12.36
FeO	16.14	13.96	19.07
MnO	BD	0.02	BD
MgO	BD	0.07	0.02
CaO	6.05	2.31	3.24
Na_2O	2.86	2.95	2.58
K_2O	5.50	6.03	5.58
BaO	0.09	0.04	0.10
ZnO	0.08	0.05	0.08
Cl^-	0.10	0.05	0.07
Cr_2O_3	0.05	BD	BD
NiO	BD	BD	BD
V_2O_3	0.02	0.04	0.00
SO_3	0.66	0.44	5.15
CuO	0.12	0.05	0.52
P_2O_5	1.67	0.52	0.00
Total	96.02	93.10	93.37

6.4.4. Spinel oxides

Spinel and other iron oxides are found in smaller proportions in the slags studied. Spinel form mainly well-confined rounded shape, euhedral to subhedral small crystals (mostly 10 μm/0.01 mm) mainly occurs as inclusions in olivine. Due to its small sizes spinel was difficult to analyse by microprobe. Crystals of spinel are visible at **Fig. 11 and 12.** The ratio of X_{Mg} ($Mg/(Mg+Fe^{2+})$) from 0.04 to 0.15, the ratio of X_{Cr} ($Cr/(Cr+Al)$) showing that the Cr is one of the main components in the spinel, ranging from 0.81 to 0.91, and the ratio of $Fe^{2+}/(Fe^{2+} + Fe^{3+})$

Table 6: Microprobe spinel analyses of slags from al-Ṣalaylī, Oman (wt.%; recalculated for a.p.f.u; BD, Below the detection limit)

Sample	A	A	B
Num.	28.00	29.00	45.00
SiO_2	0.5249	0.1855	0.4003
TiO_2	0.3304	0.2432	0.7418
Al_2O_3	4.41	3.66	2.97
MgO	0.6486	1.7410	2.7575
FeO_{tot}	58.84	55.25	44.75
MnO	0.0588	0.0568	0.0720

CaO	0.6182	0.3324	0.1328
Cr_2O_3	27.77	32.04	44.25
V_2O_3	0.1500	0.1105	0.1581
ZnO	0.1216	0.1206	0.0912
NiO	BD	0.0456	0.0426
CuO	0.2503	0.4388	0.2392
BaO	BD	BD	0.0730
Na_2O	0.0294	BD	BD
K_2O	0.0233	0.0395	0.0527
P_2O_5	BD	BD	0.0466
SO_3	BD	BD	0.0902
Cl^-	BD	0.0101	0.0182
Total	93.9	94.31	96.89
O	4.00	4.00	4.00
Si	0.0198	0.0070	0.0147
Ti	0.0094	0.0069	0.0205
Al	0.1965	0.1619	0.1284
Mg	0.0365	0.0975	0.1507
Fe^{2+}	0.9547	0.8822	0.8698
Fe^{3+}	0.9047	0.8538	0.5023
Mn	0.0019	0.0018	0.0022
Ca	0.0250	0.0134	0.0052
Cr	0.8297	0.9516	1.28
V	0.0045	0.0033	0.0046
Zn	0.0034	0.0033	0.0025
Ni	BD	0.0014	0.0013
Cu	0.0071	0.0125	0.0066
Ba	BD	BD	0.0010
Na	0.0022	BD	BD
K	0.0011	0.0019	0.0025
P	BD	BD	0.0014
S	BD	BD	0.0025
Cl^-	BD	0.0006	0.0011
Total	3.00	3.00	3.00
X_{Mg}	0.0369	0.0995	0.1477
X_{Cr}	0.8085	0.8546	0.9090
$Fe^{2+/}(Fe^{2+} + Fe^{3+})$	0.5134	0.5082	0.6339

6.4.5. Sulphides and iron oxides

Sulphides are common phases in copper metallurgical slags. Sulphides and metals occur in slags as the main metallic compounds, which are separated by liquation from a silicate melt.

Microprobe analyses were carried out in larger inclusions as well as in small droplets encased in olivine and glass. Iron oxides and copper sulphides were mainly observed in slag A, D. The most abundant sulphides in the samples examined include chalcocite, digenite, bornite, and covelline.

Table 7: Microprobe analysis of iron oxides from slag (wt.%; recalculated for a.p.f.u; BD, Below the detection limit)

Sample	A	A	A	A	A
Num.	7	8	9	10	11
Fe_2O_3	94.21	94.44	94.26	95.18	94.78
TiO_2	0.65	0.62	0.45	0.08	0.10
SiO_2	0.32	0.39	0.37	0.25	0.28
Al_2O_3	0.79	0.82	0.84	0.48	0.76
MgO	0.03	0.03	0.04	0.06	0.06
MnO	BD	BD	BD	BD	BD
CaO	0.16	0.18	0.28	0.02	BD
Cr_2O_3	0.73	0.71	0.78	0.29	0.31
V_2O_3	0.19	0.14	0.13	0.03	BD
ZnO	BD	0.07	0.09	BD	BD
NiO	BD	BD	BD	BD	BD
CuO	0.05	0.07	BD	0.56	0.46
BaO	BD	BD	BD	BD	BD
Na_2O	0.03	0.02	BD	0.03	BD
K_2O	0.03	0.02	BD	BD	BD
P_2O_5	BD	BD	BD	BD	BD
SO_3	BD	BD	BD	0.09	0.07
Cl^-	BD	BD	0.02	BD	BD
Total	97.30	97.56	97.34	97.11	96.90
O	3	3	3	3	3
Fe^{3+}	1.92	1.92	1.92	1.95	1.94
Ti	0.01	0.01	0.01	0.00	0.00
Si	0.01	0.01	0.01	0.01	0.01
Al	0.03	0.03	0.03	0.02	0.02
Mg	0.00	0.00	0.00	0.00	0.00
Mn	BD	BD	BD	BD	BD
Ca	0.00	0.01	0.01	0.00	BD
Cr	0.02	0.02	0.02	0.01	0.01
V	0.00	0.00	0.00	0.00	BD
Zn	BD	0.00	0.00	BD	BD
Ni	BD	BD	BD	BD	BD
Cu	0.00	0.00	BD	0.01	0.01
Ba	BD	BD	BD	BD	BD
Na	0.00	0.00	BD	0.00	BD
K	0.00	0.00	BD	BD	BD
P	BD	BD	BD	BD	BD
S	BD	BD	BD	0.00	0.00
Cl^-	BD	BD	0.00	BD	BD
Total	2.00	2.00	2.00	2.00	2.00

6.4.6. Other phases

In addition to the primary and secondary phases described above, other secondary phases of minerals occur in the examined slags. Minerals such as albite, chrysotile, bornite, pyrrhotine, chromite, anorthite, diopside and chalcopyrite. Grain of silver was found in sag D.

6.5. Radiocarbon dating

With the radiocarbon method, we can reconstruct periods younger than 55000 years. Most prehistoric mines in Europe and the Near East have been dated through the radiocarbon (Hauptmann, 2007). This method is suitable for nearly all kinds of metallurgical activities because of the fact that the fuel materials was wood and charcoal (Hauptmann, 2007), which could remain enclosed in slag. When the polished thin sections were made, carbons/charcoals? were found in the slag D, which were subsequently removed by drilling (**Fig. 21**). This material was sent for analysis by the radiocarbon (^{14}C) method. Raman spectrometry showed a superior presence of manganese oxide than carbon.

The total weight of the analysed sample before the pre-treatment was 0,0303 g. A standard acid-base-acid method was used for purifying the sample and removing possible contaminants. After purification the amount of the sample was 0,0001 g. Unfortunately, this amount of recovered material was not in sufficient quantity for radiocarbon dating method to be successful, which was demonstrated by the low pressure after converting the sample to CO_2.

6.6. Remote sensing

The remote sensing method which uses satellite imagery to map archaeological slag heaps is efficient to use in aridic environments with minimal vegetation cover (Sivitskis et al., 2019). The climate in Oman can be generally considered as aridic and semi-aridic, but it is changing through the different regions (Giardino, 2017). This means it can be applied in al-Ṣalaylī. Sentinel hub was used for copper mapping, which unfortunately does not use Worldview-3 imagery and its resolution is not 1 m but 10–20 m. Sentinel hub EO Browser (powered by ESA v3.28.1., Sentinel-2 L2A, Show L1C) showed copper when using slightly changed bands which is sentinel referring for "Geology" as combinations of bands R: B12, G: B11, B: B8; and R: B08, G: B11, G: B12; R: B08, G: B12, B: B02, but it did not only show copper, but also settlement and other modern human encroachments on the landscape, which would be more difficult to remove and filter out, it could be ignored, but therefore the results obtained are from my point of view unusable and should be processed better in GIS. Howari et al. (2020) used Landsat 8 (OLI) to map copper mineralisation in Oman with bands combination R: band 7, G:

band 6, B: band 2), result was not clear as can be seen in **Fig.** 1**5** when it was used for our area. But bands combination R: band 7, G: band 4, B: band 2, which was used by Howari et al. (2020) for highlight geological features where colour variation was corresponding to serpentinized peridotite, gabbro and metamorphic sole, our **Fig. 15** using this band combination showed the best result of something that can be the slag fields. Same combination of bands (R: B07, G: B04, B: B02) was used by Hajibapir et al. (2014) for exploration of hydrothermal alteration Associated with copper mineralisations mapping Kehdolan Area (Eastern Azerbaijan Province-Iran). In a—Ṣalaylī case could be B02 replaced by B01 and B03 showing very similar results. Mohebi et al. (2015) used band ratio R: B04, G: B06, B: B08 showing the distribution of Cu deposits and prospect area around Hanza Mountain also in Iran. Using different indexes ((A-B)/(A+B)), for example with A=B08, B=B02, A= B08, B= B03, A= B08, B= B04 or A= B07, B= B04 were possibly slag field coming out. Better results were observed using indexes (A/B) as B02 or B04/ B07, B02/ B08 or B04/ B08 with best result.

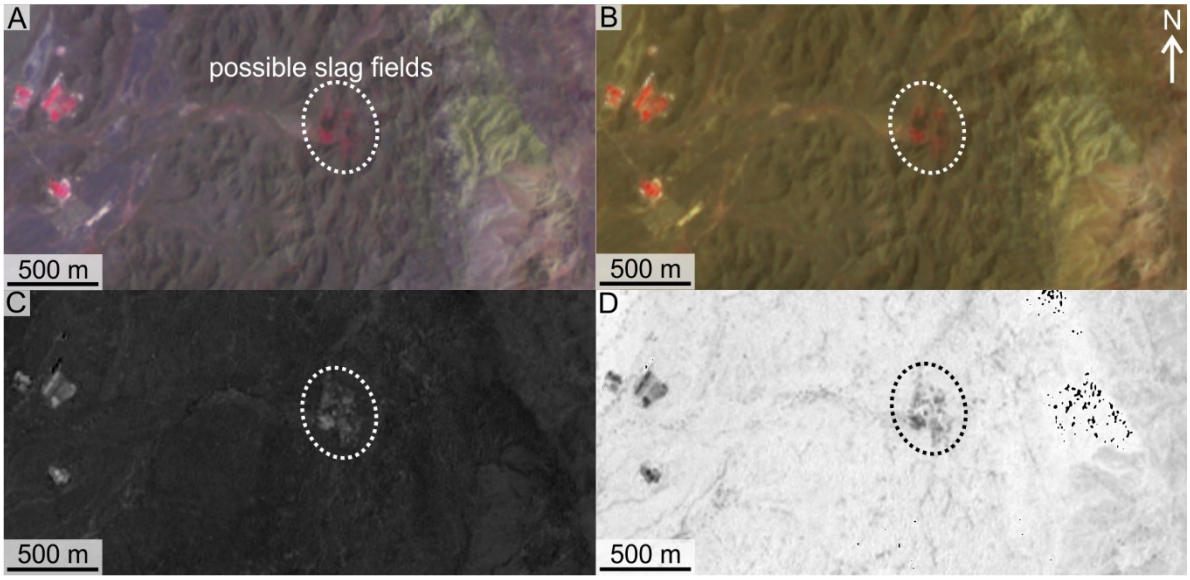

Figure 15: Area with the possible slag field is marked in circle on 22.929235, 58.288208; A - red colour in circle (band combination R: B08, G: B04, B: B12); B - red colour in circle (band combination R: B07, G: B04, B: B02); C – lighter colour in the circle (index (B08-B03)/(B08+B03)); D – darker area in the circle (index B04/B08)

7. Discussion

Slags are carriers of “DNA” of metallurgical processes in which they were formed, thanks to their mineralogical and chemical composition it is possible to reconstruct the raw materials, the conditions of operation of the smelting furnaces in which they were formed and the efficiency of metal extraction (Piatak and Ettler, 2021). This informations are especially useful for archaeologist and archaeometallurgists investigating prehistoric metal production areas (Charlton et al., 2010; Chirikure and Bandama, 2014; Piatak and Ettler, 2021). The literature is often mostly devoted to slag collected from surface, which are much more frequently studied than those obtained from excavated archaeological probes. Fortunately, nowadays is slag material approached more precisely than in the past and more geochemical analyses, simply belonging not only to metallurgical artefacts, enter the frequently purely archaeological description of the samples. Nevertheless, from some areas, this approach and insistence is missing. It is indeed important to use a more comprehensive approach of analytical methods to connect the overall context, which in the chemical composition of the slags may reflect the social situation of ancient civilisations and help to reveal the background of metallurgical processing behind slags and it is even possible to find out where else the ore could have been used. Omani slags usually do partly reflect origin of ore from which they were made (Pracejus and Scharf, 2020). Pyrometallurgical slags are by-products, waste materials of anthropogenic origin resulting from the metallurgical copper smelting process (Piatak and Ettler, 2021). Slags were indeed taken as waste and not as a valuable source of information.

The overall chemical and mineralogical composition of historical slags are mainly influenced by the composition of the source ore, the fluxes added, the type of flux and the rate of cooling time of the melt. The content of the main components can vary considerably depending on where the slag was taken, the duration of the process in which slag was made, and the point that the craft and its processes have changed over time (Hauptmann, 2007).

The fact that studied slags are result or copper metallurgy is indicated not only by the location with a rich history of copper mining and processing, but also by the elevated copper content in the samples detected from the analyses carried out. Content of copper in slags A, B and C was from 3920 mg/kg to 26050 mg/kg, we can compare it with slags from Trentino that have 5000 to 20000 mg/kg (0,5 to 2 wt.%) of copper trapped in slags (Pearce et al., 2021). In our examined slags was pure copper present, but in another Omani surface slags copper could be detected only together with iron and sulphur (Franklin et al., 1976). As these slags lack the finding

context associated with the time classification, we lack some information. The most frequently used archaeological dating approach used on slag material is slag typology based on visible changes to the slag's appearance pointing to period in which the slag was created (Peters et al., 2017). Slags can also reflect varying socio-economic and political dynamics in the region as was shown by correlation between the location of slag deposits and their interfered ages retrieved via reconstructing of their ancient geomagnetic intensities (Peters et al., 2017). For older periods geomagnetic field reconstruction depends on the presence of geological and archaeological materials with preserved remanent magnetization, which, for example occurs in the last phase of slag melt cooling, this method was frequently used to date slags from South Levant but can have erroneous results due to slag recycling at one site (Ben-Yosef et al., 2008, 2016). Phase content and bulk chemistry composition of tap slag that were frozen during tapping would therefore be the main sources of information for reconstructing of the parameters of the smelting processes (Hauptmann, 2007). It is also possible to date slags based on XRF data with determinating of technological level by comparing the results of the XRF slags analysis from similar localities with samples properly dated for example with ^{14}C method (Shilstein et al., 2020). But sadly, there are not many analyses and properly dated slags from Oman to compare obtained results.

Focusing on olivine crystals, can be key to reconstructing the melting temperature and cooling time of the slag. The growth zoning is frequently shown by olivine, which is non-equilibrium feature typical of solid solution crystals evolving under fluctuating temperature conditions (Addis et al., 2016). The flexible morphology of olivine crystals in slag can indicate different cooling paths of numerous samples from almost instant to long period of several hours before complete crystallization (Kierczak and Pietranik, 2011; Ettler et al., 2009b). Crystallisation temperature of olivine can be significantly shifted by occurrence of other chemical components such as Ca, Al and Si which may decrease the crystallization temperature of fayalite-rich olivine by up to 100 °C, but for example presence of trivalent iron which is indicated by the occurrence of magnetite in the slag, does not significantly affect the calculated temperatures (Morton and Wingrove 1969, 1972).

As can be seen on the ternary diagram (**Fig. 16**) the melting temperature was reconstructed relatively as typical for old metallurgical slags. From ternary diagram (Osborn et Muan, 1960) in slag sample A the melting temperature was lowest, approximately 1100 °C, slag B reached around 1120 °C and slag C melting temperature was about 1200 °C. On similar Omani surface slag analysed by Franklin et al. (1976) was melting temperature established at 1200 °C or more.

Due to Addis et al. (2016) minimum temperature for melting conditions is of ~1200–1250 °C. As he also tried to construct ternary diagram with his own LBA slag samples from the Luserna (Italy), the temperature was in the range 1100–1150 °C. Since this diagram is simplified, Addis et al. (2016) pointing out the fact that diagram does not consider the MgO component, and these temperatures should be considered as minimum crystallization temperatures. Slag D was by visage in section very similar to slag cakes from the 3rd millennium BCE, from Trentino near Luserna in Italy (Pearce et al., 2021).

But as is referred by Hauptmann (2007) that ancient smelting furnaces were limited and could barely ever reach temperatures much above 1200 °C. Exactly lower melting temperature could be achieved by correctly added components which influence this temperature of slag melting during gradual heating from the first liquefying of the elements at lower temperatures to achieve liquefaction of the ore charge (Hauptmann 2007). At 600–800 °C a charge consisting of SiO_2, CaO, Al_2O_3, Na_2O, P_2O_5, Cu_2O and Fe oxide, chlorides, and sulphates in a variety of mineralogical components already starts melting (Hauptmann 2007). This might be used at Faynan in Jordan exanimated by Hauptmann. For early smelting processing might be valid principle of liquation where during smelting Cu-As-ores could also form liquid alloy at around 900 °C, or just above 1000 °C during formation of metallic copper and Cu sulphite (Hauptmann 2007). Due Hauptmann et al. (2003) in EBA slag from Shahr-i Sokhta (Iran), was observed melting at temperature as low as 813 °C because of occurrence of copper-rich sulphite such as covellite (CuS). Furnace that could accomplished such roasting and smelting operations were used in Timna when it was under Roman administration and did not change in post Roman times all over the Near East (Franklin et al., 1976). In studied slag by Jesus (1976) from Ankara group, Anatolia, was found iron prills that were interpreted as not so common feature even if iron content is normal in slag. It can be explained as high temperatures engaged in smelting of the copper and might have at the same moment smelted the iron in the gangue or flux and it must mean that the temperature reached at least 1000 °C (Jesus, 1976).

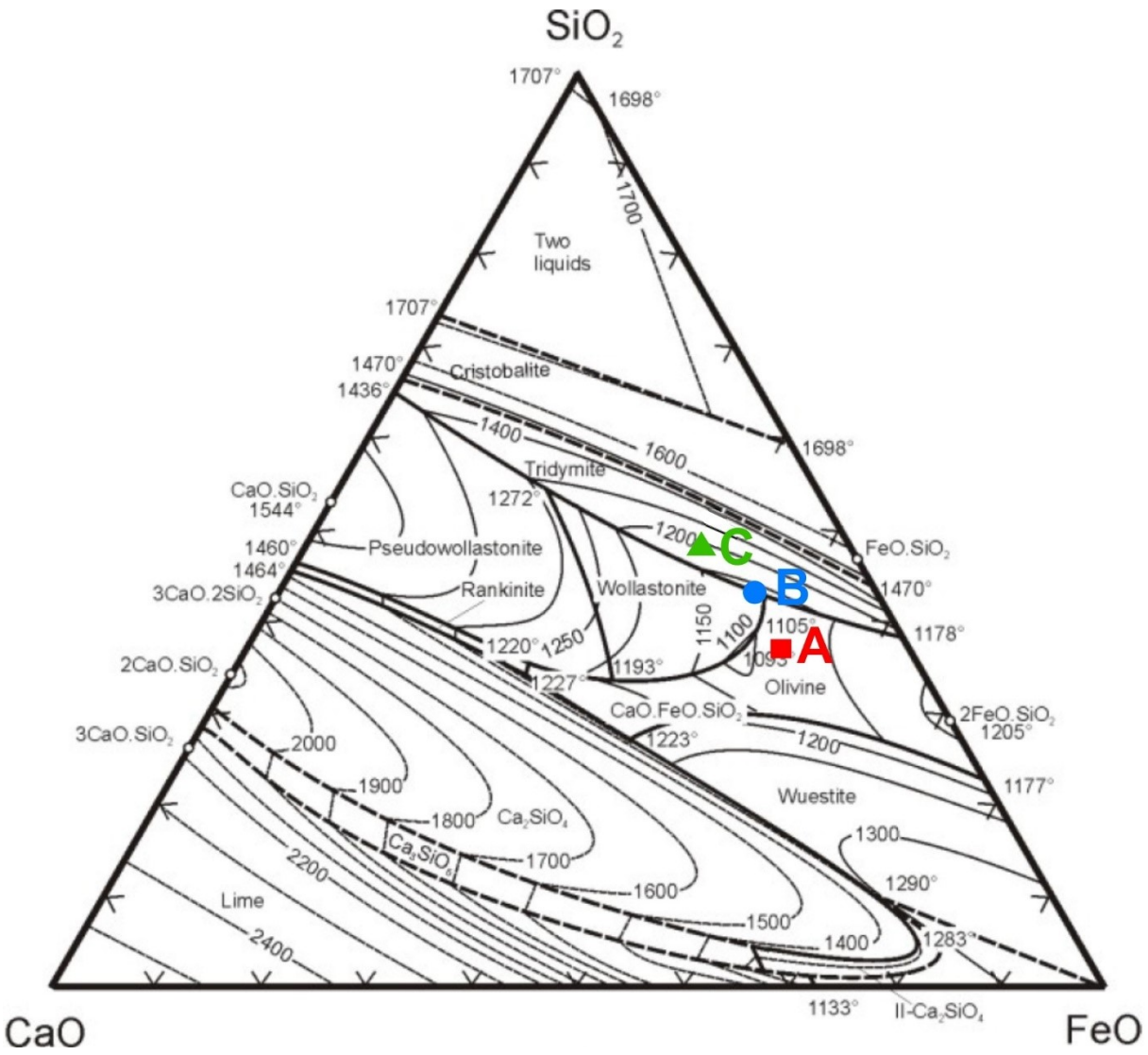

Figure 16: Ternary diagram of SiO2-CaO-FeO system for determining the melting temperature of the slag melt (according to Osborn and Muan, 1960)

Cooling temperature of slag by shape of crystals

Very distinct feature of olivine crystals is their texture which can represent and reflect various cooling temperatures and conditions (Faure et al. 2003, 2007). For interpretation and reconstruction of cooling temperature due to the shape of olivine crystals was used chart after Donaldson (1976) at **Fig. 18** and Addis et al. (2016) at **Fig. 17**, both was used as inspiration and as template for method of displaying crystals of olivine from slags from this thesis in **Fig. 19**, where you can see sketches of olivine crystals from al-Ṣalaylī slags. In Donaldsons (1976) experimental studies thanks to shape of olivine we can established cooling temperatures as you can see in **Fig. 18**. With the knowledge that these slags were tapped, they should be air cooled. It can be assumed that upper parts of slags were cooled rapidly when they came into contact

with the air, the formation of copper and prismatic olivine crystals may take about 90 and 180 hours (Addis et al. 2016). Considering sizes of crystals and their shape we can presume that the corners of slag could be part of quicker process of cooling than the middle of the slag. Analogous phenomenon of chilled edge is in nature typical for example in pillow lavas. As could be seen at **Fig. 19** different slags have olivine crystals grouped in different parts of picture, which can mean different cooling temperatures. The size of the crystals is not accurately shown in the drawing, the emphasis is mainly on their shape. Earlier mentioned slags from Trentino had based on work of Donaldson (1976) established cooling rates of 15–40 °C per hour (Pearce et al., 2021). But Cooling rates described by Donaldsons work well only with forsterite-rich olivines and appears to be not representative for iron rich systems found in archaeological slags (Ettler et al., 2009b; Pearce et al., 2021). Ettler et al. (2009b) argue that, based on the work of Faure et al. (2003), the olivine morphology progression of fayalite occurs more quickly, with hopper-type crystals forming at cooling rates in the low hundreds of degrees per hour and chains at high hundreds of degrees per hour (Faure et al., 2003; Ettler et al., 2009b; Pearce et al., 2021).

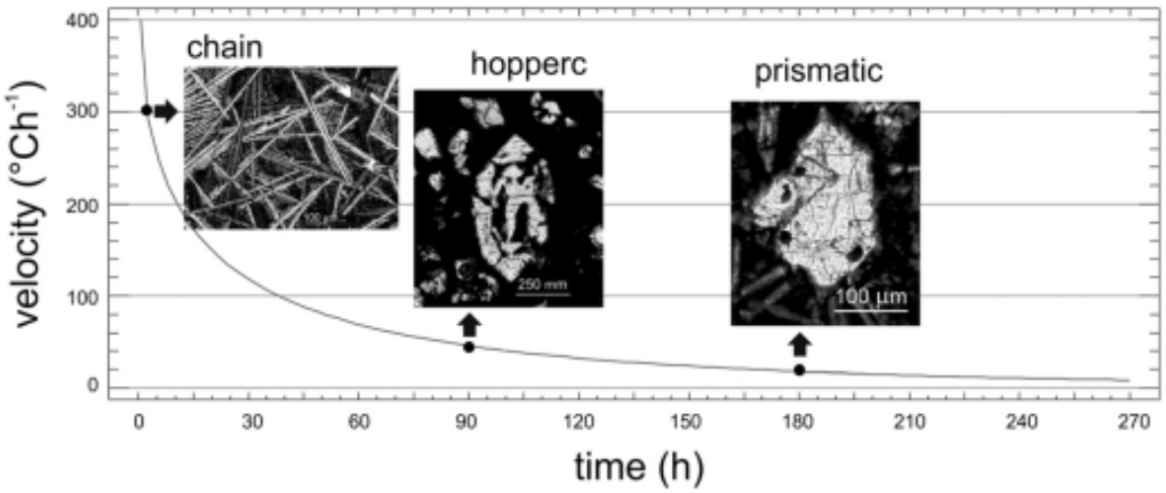

Figure 17: Slag cooling rate dependence on olivine crystal shape (Addis et al., 2016)

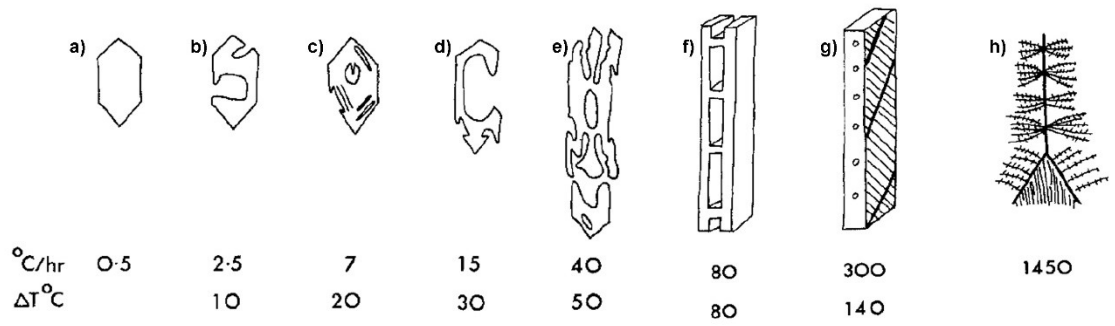

Figure 18: Olivine crystal shapes at different slag cooling rates. a) well-formed polyhedral crystal (0-5 °C/hr); b) Porphyritic olivine crystal (2-5 °C/h); c) Prismatic olivine crystal (7 °C/h); d) Porphyritic olivine (15 °C/h); e) Elongated porphyritic crystal (40 °C/h); f) H-shaped chain habitus (80 °C/h); g) Lattice crystals (300 °C/h); h) Dendritic feather-like texture (1450 °C/h) (Donaldson, 1976).

As can be seen at **Fig. 19** below, selected olivine grains from slag C (green) are gathered at left side of picture which according to Donaldsons cooling rates can mean that slag C had the most slowest cooling rate from all examined slags around 0,5 to 5 °C per hour near to equilibrium crystallisation, close to the melting point, with well-formed confined grains of olivine. In slag A there is two types of olivine crystals in sketch picture below, red crystals with average cooling rate about 7–20 °C per hour and dark red porphyritic crystals from cooled rim with average cooling rate around 15–40 °C per hour, which tells a lot about how this slag was formed. Blue olivine crystals in image represents slag B which had relatively faster cooling rate approximately 40–80 °C per hour. The previous samples were tap slags with a very high olivine content, but slag D consists mainly of other phases and its olivine crystals correspond to cooling at 80 °C per hour and higher, but probably this method cannot be applied unambiguously to this sample.

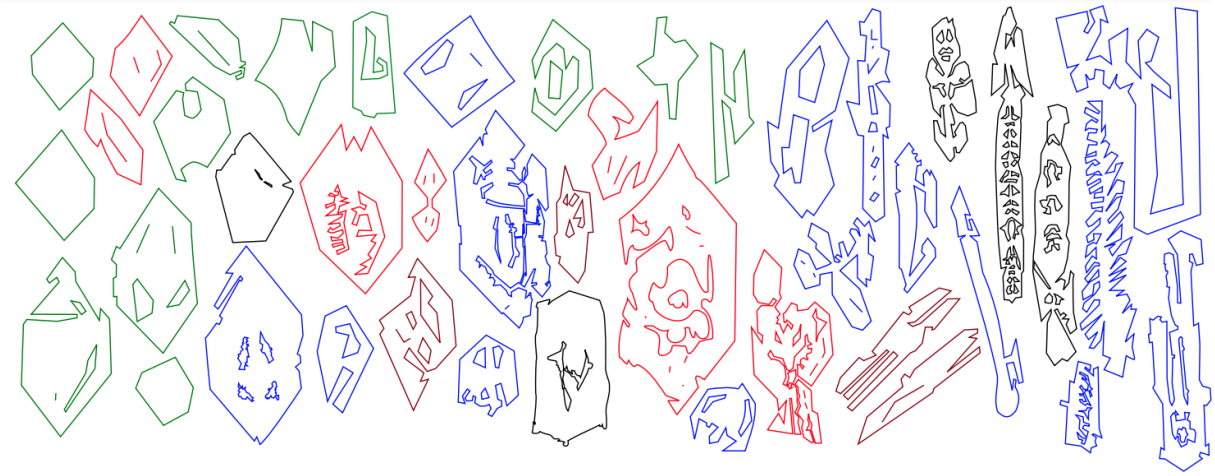

Figure 19: Sketch of olivine crystals from the examined al-Ṣalaylīs slags; slag A- red, from the cooled edge of slag - dark red; slag B -blue; slag C- green; slag D - black

In general, the finding situation is very important for the correct interpretation of archaeological finds context. For a better understanding of the results of the analyses and for the possibility of comparison, experimental archaeometallurgical experiments could be carried out in the future on ore material from local mines to verify the different melting processes and the temperature that must be reached during the metallurgical process. In the following research can be also provided lead isotope analysis. Slag can also be dated by optically stimulated luminescence (OSL) dating which is provided by measuring of time since grains of minerals (naturally occurring in sediment or man-made materials) was deposited and shielded from further light or heat exposure (Huntley et al. 1985; Aitken 1998; Bluszcz, 2004). This OSL method can determine the date of fired materials if its temperature reaches at least 400-500 °C, and it contains quartz grains or also for sediment around objects (Bluszcz, 2004). By applying thermoluminescence (TL) method to quartz crystals slag can be efficiently dated which needs to be separated from the slag (Haustain et al., 2003). Precious archaeological material which can be dated using TL method are furnace remains and their fragments (Zacharias et al. 2006). Determining cooling temperature is important also for reconstructing archeointensity of copper slag as was shown by Ben-Yosef (2008) and establishing the period of time when slag was made. This method can be used in future at al-Ṣalaylī site if, for example, a furnace with slag in situ. For my diploma thesis I need to collect material from the excavated test pit at the site, which would be suitable for further investigation with a better archaeological context, ideally slags with sealed charcoal residues from the production for successful ^{14}C dating and further analyses.

8. Conclusion

The results showed that from the mineralogical point of view, the studied slags are mainly composed of olivine and clinopyroxene series silicates, glass and, to a lesser extent, spinel-type oxides. Small amount of protolith minerals (lizardite, talc) can be preserved. Sulphides are mainly represented by chalcocite and covelline. Metallic copper forming inclusions in the matrix is also common. A number of alteration products (Fe-oxides, cuprite, brochantite) indicate weathering processes at the site. According to the SiO_2-CaO-FeO ternary diagram, the melting temperature of the slags was close to 1200 °C. The process of crystallization and solidification was very rapid for the slag D, as shown by the skeletal shapes of the crystals and the presence of glass and slower for other slags. The Cu concentrations in the slags (3920 to 26050 mg/kg) and the relatively high viscosity index documenting the low viscosity of the slag melt indicate the high efficiency of ancient metallurgical processes at this site. Thanks to the analyses carried out and the results obtained, it has been confirmed that slags A, B and C are tapping slag. Copper mining and processing into bronze metal objects influenced not only the eastern world and Anatolia, but also had an impact on European trade. Isotope analyses can direct the subject to the deposit from which the source ore was extracted. But a more precise answer can only be given after elemental analyses and a more precise dating, how much this contact influenced the world is an open question. The extent of the copper that was mined can be shown by remote sensing methods and this range can be refined by more precise methods in further research. Remote sensing is a very good non-destructive tool for mapping ore deposits and even slag fields, but it can also help to discover previously undiscovered metallurgical undiscovered places in much more detail. By combining multiple methods together, it can show the problem from multiple angles, and we are able to better define the metallurgical processes. Dating is the key to recognising the different stages of metallurgical development in a given area. Older slags were produced using less developed technology and, thanks to progress, it is possible to trace the gradual improvement and development of metalworking technology. It is a very good tool for the recognition of the typology in archaeological areas. Accurate dating of the slags from the excavated probe would not only help with the dating of the metallurgical processes itself but also with a much larger range of objects related to them. Samples for my further investigations at this site will be obtained thanks to my newly established collaboration with Gaudiello, who won the Beatrice de Cardi award.

9. References

Addis A., Angelini I., Nimis P., Artioli G., 2016: Late Bronze Age copper smelting slags from Luserna (Trentino, Italy): Interpretation of the metallurgical process. Archaeometry, 58, 96-114.

Aitken M. J., 1998: Introduction to optical dating: the dating of Quaternary sediments by the use of photon-stimulated luminescence. Oxford: Oxford University Press.

Allaby M., 2013: A Dictionary of Geology and Earth Sciences (4 ed.), Oxford

Almazroui, M., 2012: Recent climate change in the Arabian Peninsula: Seasonal rainfall and temperature climatology of Saudi Arabia for 1979–2009. Atmospheric Research 111: 29-45. Elsevier.

Bachmann H. G., 1982: The identification of slags from archaeological sites in situ of archaelogy, occasional publication No.6, University of London, UK.

Bamberger M., Wincierz P., Bachmann H.G., Rothenberg B., 1986: Archaeological evidence at Timna and experimental approach. Metall, 40, 1166-1174.

Begemann, F., Hauptmann, A. et al., 2010: Lead Isotope and Chemical Signature of Copper from Oman and its Occurrence in Mesopotamia and Sites on the Arabian Gulf coast. Arabian Archaeology and Epigraphy, 21, 135-169.

Benoist A., 2000: La céramique de l'Age du Fer en péninsule d'Oman. PhD Thesis. Paris

Ben-Yosef, E., H. Ron, L. Tauxe, A. Agnon, A. Genevey, T. E. Levy, U. Avner, and M. Najjar 2008: Application of copper slag in geomagnetic archaeointensity research, J. Geophys. Res., 113, B08101

Beránek M., Šebková J., Pendlík M., 1984. Technologie kovových materiálů. SNTL Praha, 330.

Bluszcz, A., 2004: OSL Dating in Archaeology. In: Marian Scott, E., Alekseev, A.Y., Zaitseva, G. (eds) Impact of the Environment on Human Migration in Eurasia. NATO Science Series: IV: Earth and Environmental Sciences, vol 42. Springer, Dordrecht.

Charlton, M. F., Crew P., Rehren T., Sheennan, S., J., 2010: J. Anthropol. Archaeol. 29, 352.

Chirikure, S., and Bandama, F., 2014: Archeometry 56, 296.

Cleuziou, S., and Tosi M. (eds), 2007: In the Shadow of the Ancestors: The Prehistoric Foundations of the Early Arabian Civilization of Oman. Muscat: Ministry of Heritage and Culture.

D'Amico, C., Gasparotto, G., Pedrotti, A., 1998: Scorie eneolitiche di Gaban e Acquaviva (Trento). Caratteri, provenienza ed estrazione del metallo. In: D'Amico C, Albore Livadie C (eds) Le Scienze della Terra e l'Archeometria. Pubblicazioni dell'Istituto Suor Orsola Benincasa. CUEN, Naples, pp 31–38

Dilek, Y., Furnes, H., 2009: Structure and geochemistry of Tethyan ophiolites and their petrogenesis in subduction rollback systems. Lithos 2009, 113, 1–20.

Donaldson, CH., 1976: An experimental investigation of olivine morphology. Contrib Miner Petrol 57:187–195

Dungworth, D., 2012: Archaeology Datasheet 202: Copper: smelting and production of alloys. The Historical Metallurgy Society.

Ettler, V., 2000: Etude du potential polluant de rejects anciens et actuels de la métallurgie du plomb dans district de Příbram. Dissertation Work, Orléans, 304.

Ettler, V., Johan Z., Kříbek B., Šebek O., Mihaljevič M., 2009a: Mineralogy and environmental stability of slags from the Tsumeb smelter, Namibia. Appl. Geochem., 24, 1-15.

Ettler, V., Červinka, R., Johan, Z., 2009b: Mineralogy of medieval slags from lead and silver smelting (Bohutin, Příbram district, Czech Republic): towards estimation of historical smelting conditions. Archaeometry 51, 987-1007.

Ettler, V., Johan, Z., Zavrel, J., Selmi, M., Wallisova, K., Mihaljevič, M., Šebek, O., 2015: Slag remains from the Na Slupi site (Prague, Czech Republic): evidence for early medieval non-ferrous metal smelting

Faure, F., Trolliard, G., Nicollet, C., and Montel, J. M., 2003: A developmental model of olivine morphology as a function of the cooling rate and the degree of undercooling, Contributions to Mineralogy and Petrology, 145(2), 251–63.

Faure, F., Schiano, P., Trolliard, G., Nicollet, C., and Soulestin, B., 2007: Textural evolution of polyhedral olivine experiencing rapid cooling rates, Contributions to Mineralogy and Petrology, 153(4), 405–16.

Franklin, U. M., Grosjean, J.-C., Tinkler M. J., 1976: A study of ancient slags from Oman, Canadian Metallurgical Quarterly, 15:1, 29-35

Gale, N., et al. 1985: Alloy Types and Copper Sources of Anatolian Copper Alloy Artefacts. Anatolian Studies 35:143-173.

Garba, R., 2014: METALLURGY OF THE NEAR EAST: Sources, Production and Distribution of Copper-Alloy Objects in the Early Iron Age of South Eastern Arabia. BA thesis. University of Leicester.

Gaudiello M., and Yule, P. A., 2017: Photogrammetric recording of an Early Iron Age hut tomb in central Oman

Gaudiello, M., and Yule, P. A., 2018: Survey in Wadi Musfah, east of Ǧebel al-Ṣalayli, Sharqiyyah north province (Sultanate of Oman)

Gaudiello, M., and Yule, P. A., 2019: Study visit to Oman 28.03–12.04.2019 Heidelberg University team

Ghazanfar, S. A., 1992: Quantitative and Biogeographic Analysis of the Flora of the Sultanate of Oman. Global Ecology and Biogeography Letters, Nov., 1992, Vol. 2, No. 6 (Nov., 1992), pp. 189-195

Giardino, C., and Genchi, F., 2014: New evidence from Oman: as-Safah production site and the Daba tombs. Presentation in Early Arabian Metallurgy Workshop, 26-07-2014 – British Museum, London.

Gilgen, S. A., Diamond, L. W., Mercolli, I., Al-Tobi, K., Maidment, D. W., Close, R., & Al-Towaya, A., 2014: Volcanostratigraphic controls on the occurrence of massive Sulfide deposits in the Semail ophiolite, Oman. Economic Geology, 109(6), 1585–1610.

Hacker, B. R., Mosenfelder, J. L., Gnos, E., 1996: Rapid emplacement of the Oman ophiolite: Thermal and geochronologic constraints. Tectonics. 15, 1230–1247

Hajibapir, G., Lotfi, M., Zarifi, A. Z., Nezafati, N., 2014: Application of Different Image Processing Techniques on Aster and ETM+Images for Exploration of Hydrothermal Alteration Associated with Copper Mineralizations Mapping Kehdolan Area (East-ern Azarbaijan Province-Iran). Open Journal of Geology, 4, 582-597.

Hauptmann, A., 1980: Islamisches Montanwesen, frühislamische Phase, in: G. Weisgerber, "5000 Jahre und Kupfer in Oman", Der Anschnitt 32, 66–73).

Hauptmann, A., 1985: 5000 Jahre Kupfer in Oman, Vol. 1: Die Entwicklung der Kupfermetallurgie vom 3. Jahrtausend bis zur Neuzeit. Der Anschnitt, Beiheft 4, 1-137.

Hauptmann, A., 2000: Zur frühen Metallurgie des Kupfers in Fenan/Jordanien. Der Anchnitt, Beiheft 11. Deutsches Bergbaum-Museum, Bochum

Hauptmann A., 2007: The archaeometallurgy of copper: Evidence from Faynan, Jordan. Springer Berlin, 308 str.

Hauptmann, A., 2020: Archaeometallurgy – materials science aspects. Natural Science in Archaeology. Springer, New York

Hauptmann, A., Rehren, Th., Schmitt-Strecker, S., 2003: Early Bronze Age Copper Metallurgy at Shahr-i Sokhta (Iran), reconsidered. In: Stöllner T, Körlin G, Steffens G, Cierny J (eds) Man and Mining – Mensch und Bergbau. Studies in honour of Gerd Weisgerber on occasion of his 65th birthday. Der Anschnitt, Beiheft 16, Deutsches Bergbau-Museum Bochum, pp 197–213

Haustain, M., et al. 2003: Dating Archaeometallurgical Slags Using Thermoluminescence. Archaeometry 45/3: 519-530.

Howari F., Ghrefat, A. H., Nazzal Y., et al., 2022: Delineation of Copper Mineralization Zones at Wadi Ham, Northern Oman Mountains, United Arab Emirates Using Multispectral Landsat 8 (OLI) Data

Huntley D. J., Godfrey-Smith D. I., Thewalt M. L.W., 1985: Optical dating of sediments. Nature 313:105-107

Jesus, P. S., 1976: Metallurgical Practices in Early Anatolia. Institute of Archaeology, London University

Khan, A. J., Botti, S., Al-Subhi, A. M., Gundersen-Rindal, D. E., Bertaccini, A. F., 2002: Molecular Identification of a New Phytoplasma Associated with Alfalfa Witches'-Broom in Oman.

Kierczak, J., Pietranik, A., 2011: Mineralogy and composition of historical Cu slags from the Rudawy Janowickie Mountains, southwestern Poland. University of Wroclaw

Mahan, A., Arfania, R., 2018: Exploring Porphyry Copper Deposits in the Central Iran Using Remote Sensing Techniques

Mahfoud, R. F., and Beck, J. N., 1997: Copper mineralizationsin the ophiolite of Oman: The genesis and emplace-ment relationship with the orogenic movements of ser-pentized peridotite. International Geology Review, 39, pp.252–286

Manasse A., Mellini M., Viti C., 2001: The copper slags of the Capattoli Valley, Campiglia Marittima, Italy. Eur. J. Mineral., 13, 949-960.

Mohebi, A., Mirnejad, H., Lentz, D., Behzadi, M., Dolati, A., Kani, A., Taghizadeh, H., 2015: Controls on porphyry Cu mineralization around Hanza Mountain,south-east of Iran: An analysis of structural evolution from remotesensing, geophysical, geochemical and geological data

Moorey, P., 1999: Ancient Mesopotamian Materials and Industries: The Archaeological Evidence. Eisenbrauns.

Morimoto, N., 1989: Nomenclature of pyroxenes. Mineralogical Journal, 14(5), 198-221.

Morton, G., and Wingrove, J., 1969: Constitution of bloomery slag. Part I: Roman, Journal of the Iron and Steel Institute, 207, 1556–64.

Morton, G., and Wingrove, J., 1972: Constitution of bloomery slag. Part II: medieval, Journal of the Iron and Steel Institute, 210, 478–88.

Osborn E.F., Muan A., 1960: Phase equilibrium diagrams in oxide systems. American ceramic society and E. Orton. Jr. ceramic foundation, Columbus, OH, USA.

Partington, G., 2009: Developing Models using GIS to Assess Geological and Economic Risk: An Example from Mineral Exploration in Oman for VMS Copper Gold Mineralisation. In: Smart Science for Exploration and Mining, Williams et al. (editors), Proceedings of theTenth Biennial SGA Meeting, Townsville, Australia, 836–838

Peake, H., 1928: The Copper Mountain of Magan. Antiquity 2, 452-457.

Peters, I., Tauxe, L., Ben-Yosef, E., 2017: Archaeomagnetic Dating of Pyrometalurgical Contexts: A Case Study for Copper Smelting Sites in the Central Timna Valley, Israel

Petrík, J., Mihok, Ľ., 2007: História hutníctva. Technická univerzita v Košiciach, Hutnická fakulta, Košice, 120.

Pfeiffer, T., Muller, S., Schiling, A., Roggendorf, H., 2012: Dissolution of copper slag glasses

Piatak, N. M., and Ettler, V., 2021: Metallurgical Slags: Environmental Geochemistry and Resource Potential. Buch, 978-1-78801-887-6.

Potts, D., 1993: Patterns of Trade in Third-Millennium BC Mesopotamia and Iran. World Archaeology 24(3): 379-402. Taylor & Francis, Ltd.

Potts, D., 1999: 'The Plant for the Heart Grows in Magan ...': Redefining Southeastern Arabia's Role in Ancient Western Asia. Australian Archaeology 48: 35-41.

Pracejus, B., and Scharf, A., 2020: Do Omani Cu-Slags Reflect the Origin of Hydrothermal Fluids? Conference: International Conference on Ophiolites and the Oceanic Lithosphere: Results of the Oman Drilling Project and Related Research, 12-14th January, 2020

Prange, M., 2001: 5000 Jahre Kupfer im Oman; Band 2: Vergleichende Untersuchungen zur Charakterisierung des omanischen Kupfers mittels chemischer und isotopischer Analysenmethoden. Metalla 8: 1–126.

Rehder, J. E., 1994: Blowpipes versus Bellows in Ancient Metallurgy. Journal ofField Archaeology 21:345-350.

Rioux, M., Bowring, S., Kelemen, P., Gordon, S., Miller, R., Dudás, F., 2013: Tectonic development of the Samail ophiolite: High-precision U-Pb zircon geochronology and Sm-Nd isotopic constraints on crustal growth and emplacement: Tectonic History of the Samail Ophiolite. J. Geophys. Res. Solid Earth 2013, 118, 2085–2101.

Rosenberg, N., 1980; Technology, Natural Resources and Economic Growth In: Economic Growth and Resources

Scharf, A., Mattern, F., Al-Wardi, M., Frijia, G., Moraetis, D., Pracejus, B., Bauer, W., Callegari, I., 2021: Tectonostratigraphy of the eastern part of the Oman Mountains

Searle, M., Cox, J., 1999: Tectonic setting, origin, and obduction of the Oman ophiolite. Geol. Soc. Am. Bull. 111, 104–122.

Shilstein, S., Tal, K.-C.-M., Avner U., Shalev, S., 2020: Detecting changes in copper technology by analyzing slag from Nahal Amram Israel

Sivitskis, A. J., Lehner, J. W., Harrower, M. J., Dumitru, I. A., Paulsen, P. E., Nathan S., Viete, D. R., Al-Jabri, S., Helwing, B., Wiig, F., Moraetis, D., Pracejus B., 2019: Detecting and Mapping Slag Heaps at Ancient Copper Production Sites in Oman

Warr, N. L., 2021: IMA–CNMNC approved mineral symbols

Weeks, L., 1997: Prehistoric Metallurgy at Tell Abraq, U.A.E. Arabian Archaeology and Epigraphy 8: 11-85. Munsgaard.

Weeks, L., 2003a: Prehistoric Metallurgy in the U.A.E.: Bronze Age–Iron Age Transitions. Proceedings of the First International Conference on the Archaeology of the U.A.E. pp 116-121. Trident Press.

Weeks, J., 2003b: Early Metallurgy of the Persian Gulf. Brill Academic Publishers, Boston.

Weeks, L., 2007: Coals to Newcastle, copper to Magan? Isotopic analyses and the Persian Gulf metals trade in Metals and Mines: studies in archaeometallurgy. Ed. by Susan La Niece, Duncan Hook and Paul Craddock. London: Archetype Publications in association with the British Museum, pp. 89-96.

Weisgerber, G., and Willis, L., 2000: The Use of Fire in Prehistoric and Ancient Mining: Firesetting. Paléorient 26/2: 131-149.

Weisgerber, G., 2007: Copper from Magan for Mesopotamian Cities, Window 7.1 in Cleuziou, S. and Tosi M. (eds), In the Shadow of the Ancestors: The Prehistoric Foundations of the Early Arabian Civilization of Oman. Muscat: Ministry of Heritage and Culture.

Yule, P. A., 2014: Cross-Roads: Early and Late Iron Age South Eastern Arabia. Harrassowitz Verlag.

Yule, P. A., Gaudiello, M., Lehner, J. W., 2021: Al-Ṣalaylī Valley in Eastern Oman, Early Iron Age Burial and Multi-Period Copper Production

Yule P. A., 2021b: Field report of the Alexander Sima, Heidelberg University Archaeological Mission to Oman, 9 September – 15 October 2021

Zacharias, N., Michael C. T., Georgakopoulou, M., Kilikoglou, V., Bassiakos, Y., 2006: Quartz TL Dating on Selected Layers from Archaeometallurgical Kiln Fragments a Proposed Procedure to Overcome Age Dispersion. Geochronometria 25: 29-35 - Journal on Methods and Applications of Absolute Chronology.

10. Supplementary materials

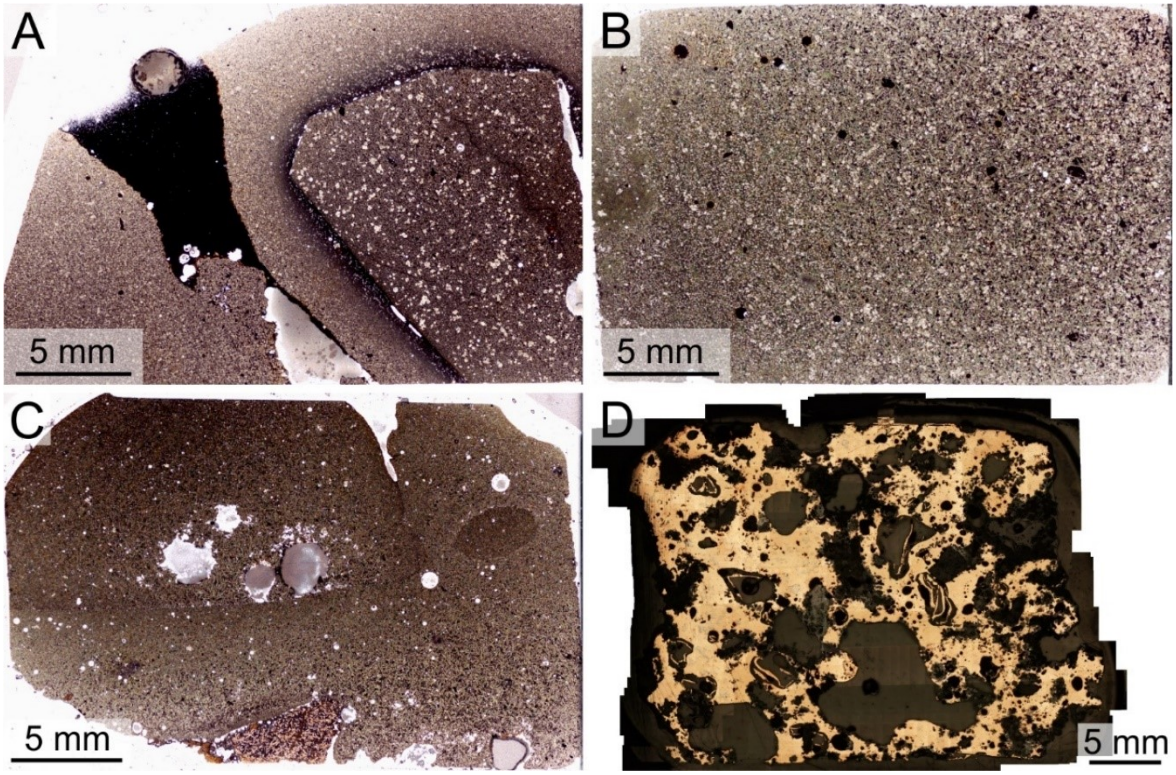

Figure 20: Thin sections scans of studied slags (Slag A, Slag B, Slag C, Slag D)

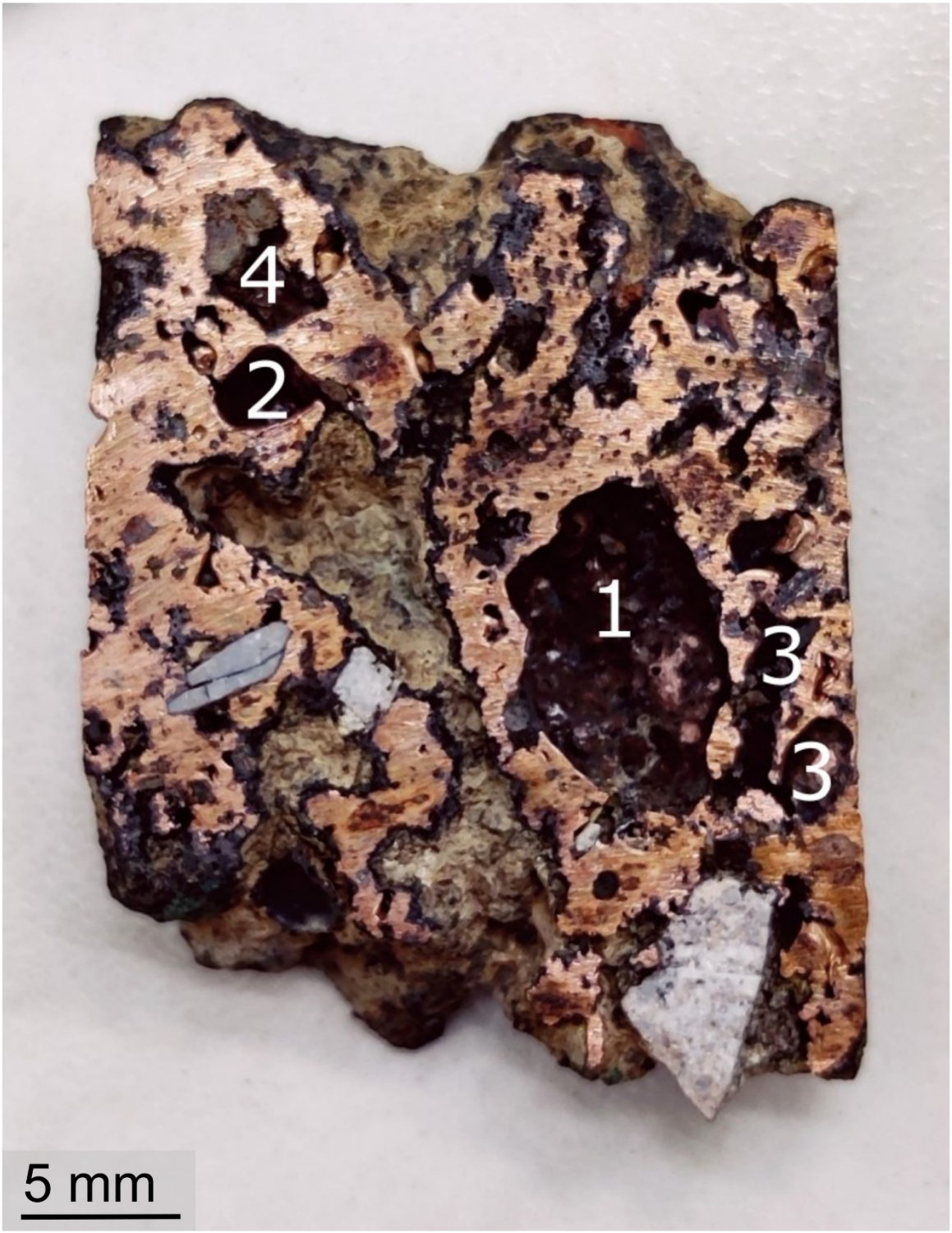

Figure 21: Drilled places with charcoals for radiocarbon dating

Figure 22:Photography of site showing settlement and slag fields (Author: Jakub Trubač)

Table 8: Detection limits from Electron Probe Micro-Analyser

all phases					average detection limit of				
comp.	Min.	Max.	Av.	Sigma	Ol	Px	Glass	Sp	Fe-ox.
Na_2O	0.009	0.012	0.011	0.001	0.011	0.010	0.011	0.011	0.010
Al_2O_3	0.015	0.018	0.017	0.001	0.016	0.017	0.017	0.017	0.017
P_2O_5	0.032	0.044	0.038	0.002	0.038	0.036	0.035	0.041	0.043
Cl^-	0.007	0.010	0.008	0.001	0.008	0.008	0.008	0.009	0.009
CaO	0.012	0.017	0.014	0.001	0.014	0.014	0.013	0.016	0.016
K_2O	0.011	0.015	0.012	0.001	0.012	0.012	0.012	0.013	0.014
SO_3	0.048	0.064	0.055	0.004	0.055	0.052	0.054	0.057	0.062
TiO_2	0.024	0.031	0.027	0.002	0.027	0.025	0.025	0.030	0.031
Cr_2O_3	0.023	0.031	0.026	0.002	0.026	0.025	0.024	0.030	0.030
V_2O_3	0.023	0.030	0.026	0.002	0.026	0.024	0.024	0.029	0.030
BaO	0.036	0.047	0.040	0.003	0.039	0.037	0.037	0.043	0.046
FeO	0.018	0.027	0.022	0.002	0.022	0.020	0.020	0.024	0.026
MnO	0.016	0.023	0.019	0.001	0.019	0.018	0.017	0.021	0.022
ZnO	0.026	0.036	0.031	0.002	0.031	0.030	0.029	0.034	0.036
NiO	0.021	0.028	0.024	0.002	0.024	0.023	0.022	0.026	0.027
CuO	0.025	0.034	0.029	0.002	0.029	0.028	0.027	0.031	0.033
SiO_2	0.024	0.029	0.026	0.001	0.026	0.026	0.026	0.027	0.028
MgO	0.011	0.015	0.013	0.001	0.014	0.013	0.013	0.013	0.013